Inhibition of CD47 expression by siRNA

To investigate the effect on phagocytosis according to the expression level of CD47, CD47 expression of NB4 cells and CD34$^+$ cord blood cells was down-regulated using siRNA. CD47 siRNA primers used were as follows: siRNA1, UAUACACGCCGCAAUACAGAGACUC and GAGUCUCUGUAUUGCGGCGUGUAUA; siRNA2, UAGAAGUCACAAUUAAACCAAGGCC and GGCCUUGGUUUAAUUGUGACUUCUA. The Nucleofector kit V and Human CD34 Cell Nucleofector kit (both Amaxa) were used to transfect siRNA and transfected NB4 cells, and lineage-depleted cord blood cells were incubated for 48 and 24 hours, respectively. NB4 cells and CD34$^+$CD38$^-$ cells were then sorted depending on CD47 expression using the FACSAria 2 cell sorter (BD Biosciences), and these cells were used for in vitro phagocytic assays to determine the phagocytic index.

Quantitative RT-PCR

Total RNA was extracted from normal and HLH BM. Reverse transcription was performed using a high-capacity cDNA reverse transcription kit (Applied Biosystems) according to the manufacturer's instructions. CD47 and control gene 18srRNA primers were obtained from Applied Biosystems. Amplification, detection, and quantification were performed with the TaqMan ABI Prism 7000 sequence detection system (Applied Biosystems). Data were calculated by the relative quantitation method ($\Delta\Delta$Ct) compared with 18srRNA as an internal control.

Measurement of cytokines by ELISA

Cytokines, including IFN-γ, TNF-α, IL-6, and M-CSF, from HLH and normal blood serum were measured with ELISA. IFN-γ was measured with the IFN-γ Quantikine ELISA kit (DIF50; R&D Systems), TNF-α was measured with the TNF-α Quantikine HS ELISA kit (HSTA00D; R&D Systems), IL-6 was measured with the IL-6 Quantikine ELISA kit (D6050; R&D Systems), and M-CSF was measured with the M-CSF Quantikine ELISA kit (DMC00B; R&D Systems).

In vitro treatment of normal HSCs with inflammatory cytokines

To evaluated the effects of inflammatory cytokines on the expression level of CD47, lineage-depleted cord blood cells were purified by negative selection using the MACS lineage cell depletion kit (Miltenyi Biotec) and cultured in 24-well dish (3047; BD Biosciences) with 300 μL of X-VIVO10 supplemented with 10% FBS and cytokines as follows: SCF (50 ng/mL; R&D Systems), M-CSF (750 pg/mL; R&D Systems), IL-6 (200 pg/mL; R&D Systems), TNF-α (20 pg/mL; R&D Systems), and IFN-γ (250 pg/mL; R&D Systems). After 24 hours of culture, CD34$^+$CD38$^-$ and CD34$^+$CD38$^+$ cells were sorted with the FACSAria 2 cell sorter (BD Biosciences), and these cells were used to determine the phagocytic index.

Statistical analysis

Statistical analysis was performed using jmp Version 9 software (SAS Institute). CD47 expression on CD34$^+$CD38$^-$ cells, CD34$^+$CD38$^+$ cells, and bulk among the groups were compared with the Dunnett test. For siRNA experiments using NB4 cells and CD34$^+$CD38$^-$ cells, phagocytic index was compared with a conventional t test. For phagocytic assays using CD34$^+$CD38$^-$ cells from cord blood cells that had been cultured with inflammatory cytokines, P values were obtained by ANCOVA. $P < .05$ was considered statistically significant.

Results

Changes in expression levels of SIRPA or SIRPA mutations do not occur in HLH patients

Several variants of the IgV domain in SIRPA (exon3 of SIRPA), where the CD47-binding site is located, have been reported in human.[26,34] We first tested the possibility that the SIRPA polymorphism may influence the development of HLH. We examined the sequence alignment of SIRPA IgV domain of 50 Japanese healthy donors. Although many polymorphisms have been reported previously in the SIRPA IgV domain,[26] we identified 2 variants (variants 1 and 2) in the present study (Figure 1A). There are 13 amino acid differences between these 2 variants as we have described,[26] and

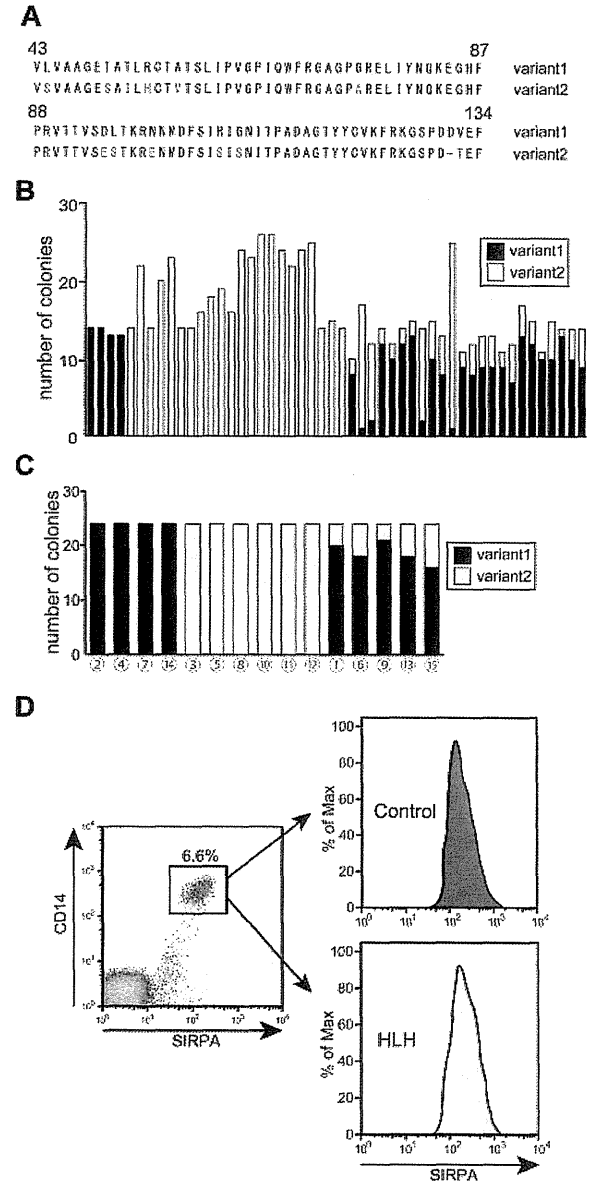

Figure 1. SIRPA mutation or changes of its expression level is not involved in pathogenesis of HLH. (A) Sequence alignment of SIRPA IgV domains (exon 3 of SIRPA) identified by sequence analysis from genomic DNA of 50 healthy donors. Two variants, which we have described previously,[20] were identified in the present study. There are 13 amino acid differences between these 2 variants. (B) Distribution of genotype of SIRPA IgV domains in 50 healthy donors. PCR products were cloned to pCR 2.1-TOPO vector and 10-25 clones were sequenced for every sample: 24 were heterozygous for variants 1 and 2, 4 were homozygous for variant 1, and 22 were homozygous for variant 2. (C) Distribution of genotype of SIRPA IgV domains in 15 HLH patients (unique patient number [UPN] 1-15); 4 (UPN 2, 4, 7, and 14) were heterozygous of variants 1 and 2, 6 (UPN 3, 5, 8, 10, 11, and 12) were homozygous for variant 1, and 5 (UPN 1, 6, 9, 13, and 15) were homozygous for variant 2. There were no other variants or changes of SIRPA IgV domain in HLH patients. (D) Representative expression of surface SIRPA on CD14$^+$ cells of control and HLH patients on FACS. There was no significant difference in the expression level of SIRPA in CD14$^+$ monocytes between HLH and normal BM: The mean $\pm$ SD of CD47 fluorescence intensity was 116 $\pm$ 1.7 and 118 $\pm$ 9.6 in healthy controls (n = 5) and HLH patients (n = 5), respectively (P = .88).

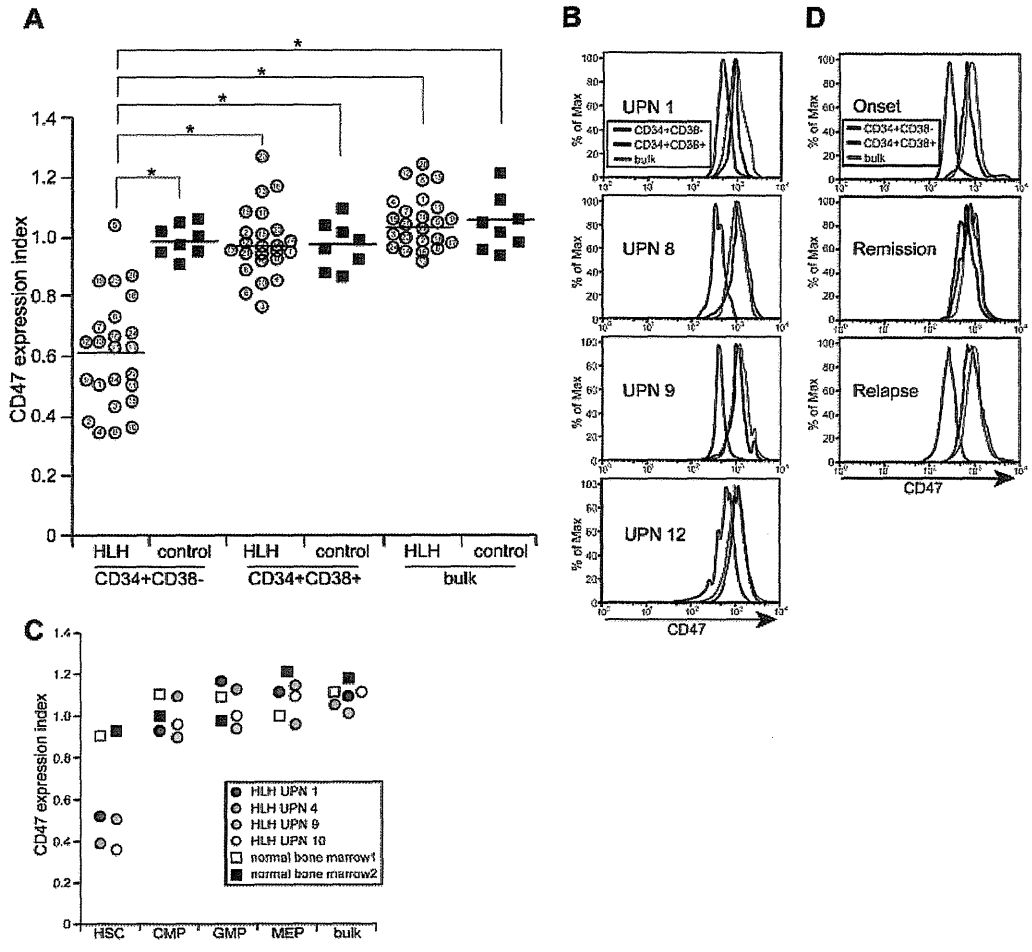

Figure 2. CD47 expression is down-regulated specifically in the CD34$^+$CD38$^-$ HSC fraction in HLH patients, reflecting the disease activity. (A) CD47 expression of CD34$^+$CD38$^-$ cells, CD34$^+$CD38$^+$ cells and unfractionated BM cells in HLH patients and healthy controls. The number in each open circle corresponds to the unique patient number (UPN) of patients (supplemental Table 1). The horizontal bars in each group show mean values of the group. The level of CD47 on CD34$^+$CD38$^-$ cells was significantly decreased compared with that on CD34$^+$CD38$^+$ cells and more mature cells. The CD47 expression index represents the relative surface CD47 level (median CD47 levels of analyzed cells/those in normal blood mononuclear cells). (B) Histograms of CD47 expression of BM cells in 4 representative HLH patients (UPN 1, 8, 9, and 12). (C) CD47 expression of CD34$^+$CD38$^-$ HSC-enriched fraction and of each progenitor cell fraction in HLH patients (UPN 1, 4, 9, and 10) and healthy controls. All progenitor populations expressed equivalent levels of CD47, and CD47 expression was down-regulated only in HSC fraction. (D) Change of CD47 expression in UPN 10 during multiple episodes of HLH. Down-regulation of CD47 repeatedly occurred at exacerbation of HLH.

their binding capacity to CD47 was equal.[34] Twenty-four of 50 healthy donors were heterozygous for variants 1 and 2, 4 were homozygous for variant 1, and 22 were homozygous for variant 2 (Figure 1B). Similarly, we examined sequence alignment of SIRPA IgV domain of 15 HLH patients, in whom we identified variant 1 and variant 2 SIRPA IgV-encoding alleles, but no other variants or changes in the allele burden of variants 1 and 2 (Figure 1C). Furthermore, the expression level of SIRPA on the cell surface did not differ among HLH and normal BM cells (data not shown) and CD14$^+$ cells (Figure 1D). These data suggest that alterations in SIRPA or its expression are not involved in the pathogenesis of HLH.

CD47 is down-regulated in the CD34$^+$CD38$^-$ HSCs from HLH patients

We also evaluated the expression level of CD47 in the BM of HLH patients. As shown in Figure 2A, the control normal BM cells ubiquitously express CD47. Its expression levels were always high in the CD34$^+$CD38$^-$ fraction that concentrates HSCs,[35] in the CD34$^+$CD38$^+$ progenitor fraction, and in unfractionated cells that mainly contained mature cells. In the HLH BM, CD47 expression is down-regulated specifically in the CD34$^+$CD38$^-$ HSC fraction compared with those in the progenitor and mature cell fraction by approximately 2-fold at the expression level (Figure 2A-B). To determine more precisely the expression of CD47 in progenitor fractions, we subfractionated CD34$^+$CD38$^+$ progenitors into common myeloid progenitor, granulocyte/macrophage progenitor, and megakaryocyte/erythrocyte progenitor populations.[29] These progenitors had equivalent levels of CD47 (Figure 2C and supplemental Figure 1). The down-regulation of CD47 occurs in conjunction with the deterioration of HLH. Patient number 10, who suffered from adult onset primary HLH due to defective PRF1,[36] had repeated episodes of HLH. The follow-up of this patient revealed that the expression levels of CD47 in HSCs normalized in remission, but its down-regulation occurred again at exacerbation of the disorder (Figure 2D). These data strongly suggest that the HSC stage-specific down-regulation of CD47 plays a critical role in HLH development.

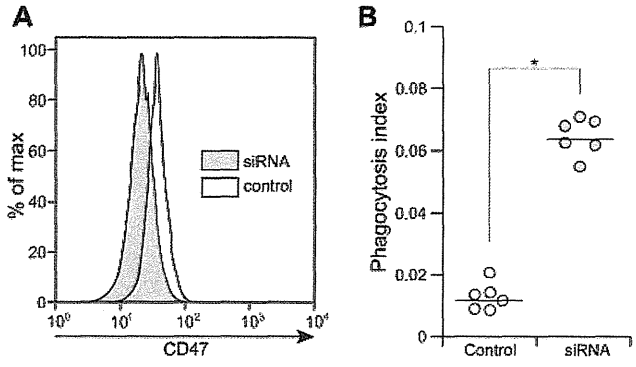

Figure 3. Knocking down CD47 in CD34$^+$CD38$^-$ cells induces their engulfment by macrophages. (A) Knockdown of CD47 expression in normal CD34$^+$CD38$^-$ cells by siRNA for human CD47. Treatment of CD34$^+$CD38$^-$ cells with siRNA for 48 hours induced 60% reduction of CD47 expression in these cells. (B) CD34$^+$CD38$^-$ cells treated with the siRNA for human CD47 showed accelerated engulfment by normal macrophages. Vertical axis shows the phagocytosis index (phagocytosis index = phagocytic macrophages/number of macrophages) and the bars show mean value. *$P < .01$ by conventional *t* test. (C) Engulfment of CD34$^+$CD38$^-$ cells treated with siRNA by normal macrophages (Giemsa staining). Scale bars indicate 10 μm.

Reduction of CD47 expression in HSCs in HLH patients results in engulfment of HSCs by macrophages

We also sought to investigate whether CD47 expression levels in target cells affect the efficiency of engulfment by macrophages. We first treated NB4, a human promyelocytic leukemia cell line, with 2 types of siRNAs targeting human CD47. siRNA1 showed a 72% reduction of CD47 expression in NB4 cells, whereas siRNA2 showed a 37% reduction (supplemental Figure 2A). We then quantitated the engulfment of macrophages by enumeration of the phagocytosis index (phagocytic macrophages/number of macrophages).[22,33,35,37] In the culture of these cells with normal macrophages, rare control NB4 cells were engulfed by macrophages, whereas NB4 cells treated with siRNA1 or siRNA2 showed 5- and 2.5-fold increases in the phagocytosis index, respectively, which illustrates the efficiency of engulfment by macrophages (supplemental Figure 2B). Therefore, the engulfment of NB4 evoked by CD47 suppression occurs in a dose-dependent manner.

We treated purified normal CD34$^+$CD38$^-$ HSCs with the siRNA1 for 24 hours and evaluated the phagocytosis index. As shown in Figure 3A, an approximately 30% reduction of the level of CD47 expression was observed in purified CD34$^+$CD38$^-$ cells treated with siRNA1. The CD34$^+$CD38$^-$ cells treated with siRNA1 became susceptible to phagocytosis, and showed 5.3-fold increase in the phagocytosis index compared with untreated CD34$^+$CD38$^-$ cells ($P < .01$). Therefore, the reduction of CD47 in CD34$^+$CD38$^-$ cells stimulates macrophages to engulf these cells.

We also investigated whether HSCs isolated from HLH patients are susceptible to phagocytosis by normal macrophages. We purified CD34$^+$CD38$^-$ HSCs and CD34$^+$CD38$^+$ progenitors from HLH patients (patients number 4, 16, and 22) and healthy controls and evaluated the phagocytosis index. As shown in Figure 4A, in all 3 HLH patient samples, CD34$^+$CD38$^-$ cells with a 40%-60% reduction of CD47 levels (Figure 2A) were actively engulfed by macrophages. In contrast, CD34$^+$CD38$^+$ cells of HLH patients showed a low phagocytic index, as was also observed in HSCs or progenitors in healthy controls (Figure 4A). Therefore, the efficiency of phagocytosis by macrophages is inversely correlated with the expression of CD47 of target cells even in human HLH samples, showing that a decrease of CD47 expression can induce engulfment of HSCs in HLH, at least in vitro.

Finally, we investigated whether HSCs were engulfed and reduced in number in HLH patients. We counted the number of CD34$^+$CD38$^-$ cells in BM from healthy controls and HLH patients (Figure 4B). The frequencies of CD34$^+$CD38$^-$ HSCs were significantly reduced in HLH BM (0.04% ± 0.02% of total nucleated cells) compared with those in normal adults (0.15% ± 0.09%). The number of nucleated cells in the BM was also reduced by approximately 50%. As a result, as shown in Figure 4B, the number of CD34$^+$CD38$^-$ cells in HLH patients was reduced down to only 23% of those in healthy adults. Although the number of CD34$^+$CD38$^+$ cells were also reduced in the HLH patients (approximately 42% of healthy adults), the reduction was more

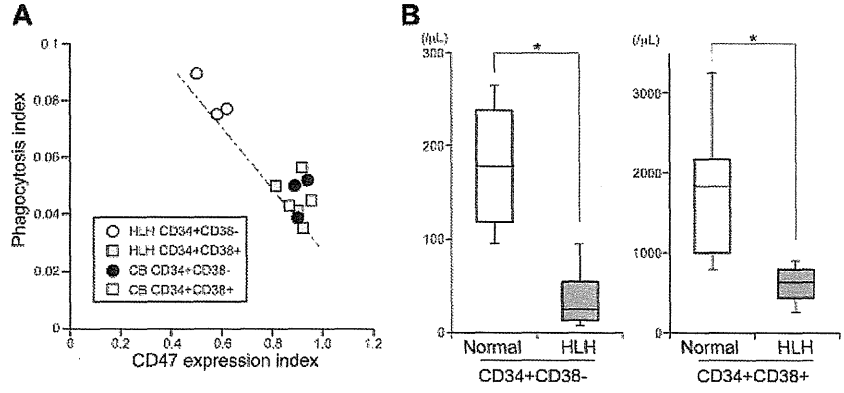

Figure 4. The CD34$^+$CD38$^-$ HSC fraction but not the progenitor population in HLH patients is sensitive to engulfment by macrophages. (A) Relationship between the level of CD47 expression and the phagocytosis index tested in vitro. CD34$^+$CD38$^-$ cells and CD34$^+$CD38$^+$ cells from 3 HLH patients (unique patient number [UPN] 4, 16, and 22) and healthy controls were cultured with activated macrophages. CD47 expression index represents the relative surface CD47 level calculated as the median CD47 levels of analyzed cells/those in normal blood mononuclear cells. The bar shows the regression line; the coefficient of correlation value was −0.91. (B) The number of CD34$^+$CD38$^-$ HSCs and CD34$^+$CD38$^-$ progenitor cells in the BM of HLH patients (n = 14) and healthy controls (n = 6) are shown in the box and whisker plot. HLH patients had significantly decreased numbers of HSC and progenitor populations, but the magnitude of suppression of HSCs was more profound. The bottom and top of the boxes are the 25th and 75th percentile values. The bands in the middle of the boxes represent the 50th percentile (median). Error bars show 1 SD differences above and below the mean of the data. *$P < .01$ by conventional *t* test.

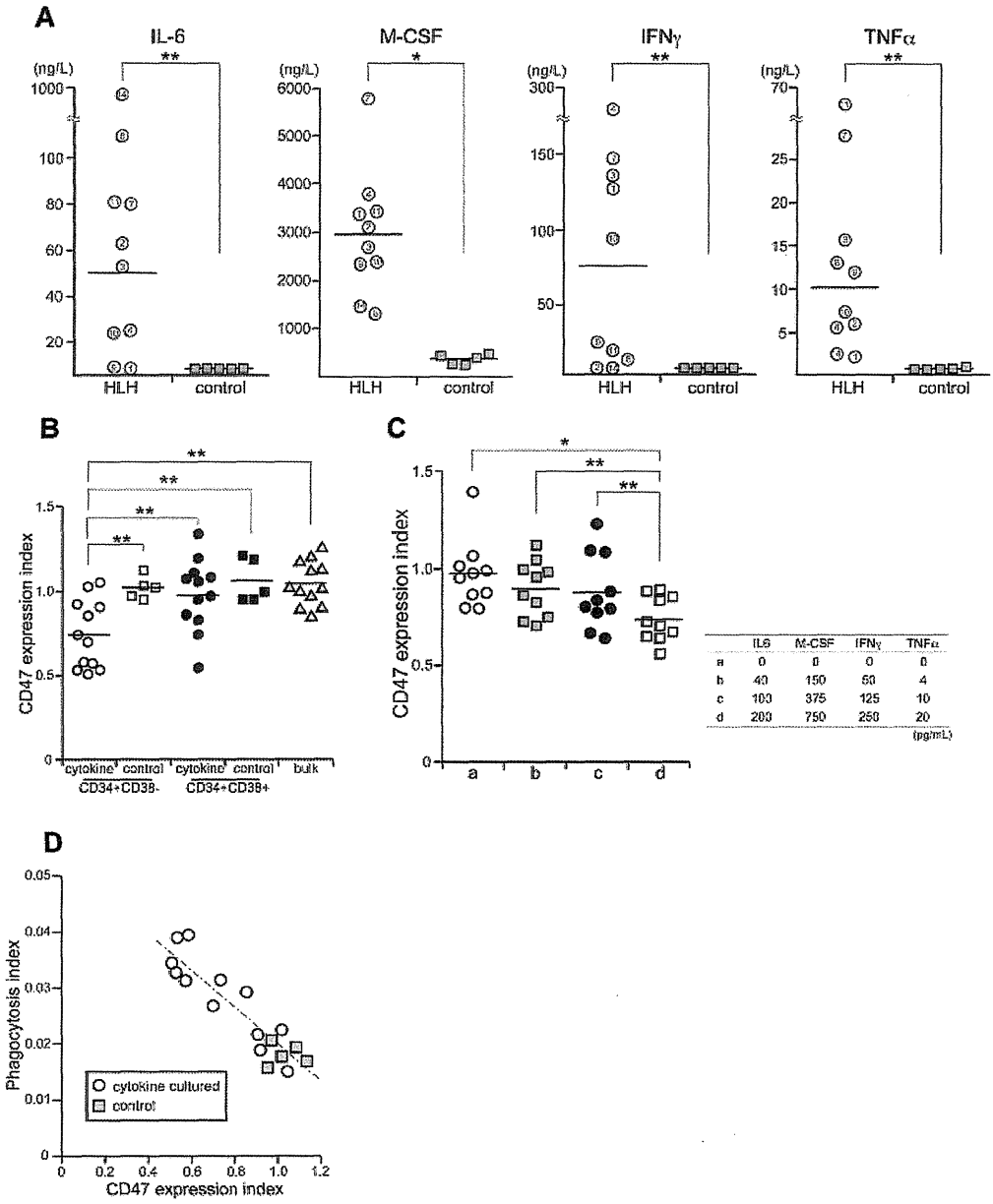

Figure 5. Inflammatory cytokines down-regulate CD47 specifically in CD34$^+$CD38$^-$ cells to induce engulfment by macrophages. (A) Serum levels of M-CSF, IL-6, TNF-α, and IFN-γ from in patients by ELISA. These cytokines were extremely high in HLH samples compared with healthy controls. *$P < .01$; **$P < .05$ by conventional t test. (B) Changes of CD47 expression levels in normal CD34$^+$CD38$^-$ HSCa and CD34$^+$CD38$^+$ progenitor cells in the presence of inflammatory cytokines. CD47 expression index represents the relative surface CD47 level calculated as median CD47 levels of analyzed cells/those in normal blood mononuclear cells. The HSC fraction, but not the progenitor fraction, showed down-regulated CD47 in response to cytokines. **$P < .05$ by conventional t test. (C) Suppression of CD47 in CD34$^+$CD38$^-$ cells by graded doses of inflammatory cytokines. The concentration of inflammatory cytokines is shown on the right. (D) Engulfment of HSCs by macrophages in response to reduction of CD47 expression by cytokines in vitro. The CD47 expression index was inversely correlated with phagocytosis index. The bar shows the regression line; the coefficient of correlation value was −0.89.

profound in the CD34$^+$CD38$^-$ fraction. The number of HSCs is reduced in the BM of HLH patient by phagocytosis that is evoked by HSC-specific reduction of CD47.

Inflammatory cytokines down-regulate CD47 expression and enhance the efficiency of engulfment of HSCs by macrophages

It has been shown that hypercytokinemia plays a critical role in the development of HLH. Consistent with previous results,[3] HLH patient sera contained high levels of inflammatory cytokines, including IL-6, M-CSF, IFN-γ, and TNF-α (Figure 5A). We investigated whether these cytokines can affect the expression of CD47 in hematopoietic cells. Lineage-depleted cord blood cells were cultured with M-CSF (750 pg/mL), IL-6 (200 pg/mL), IFN-γ (250 pg/mL), and TNF-α (20 pg/mL) for 24 hours, and CD47 expression was evaluated in stem, progenitor, and mature cell fractions. The concentrations of inflammatory cytokines were compared with those of HLH patient sera. CD47 expression was down-regulated specifically in CD34$^+$CD38$^-$ HSCs, whereas it did not change in CD34$^+$CD38$^+$ progenitors or unfractionated mature cells (Figure 5B). The down-regulation of

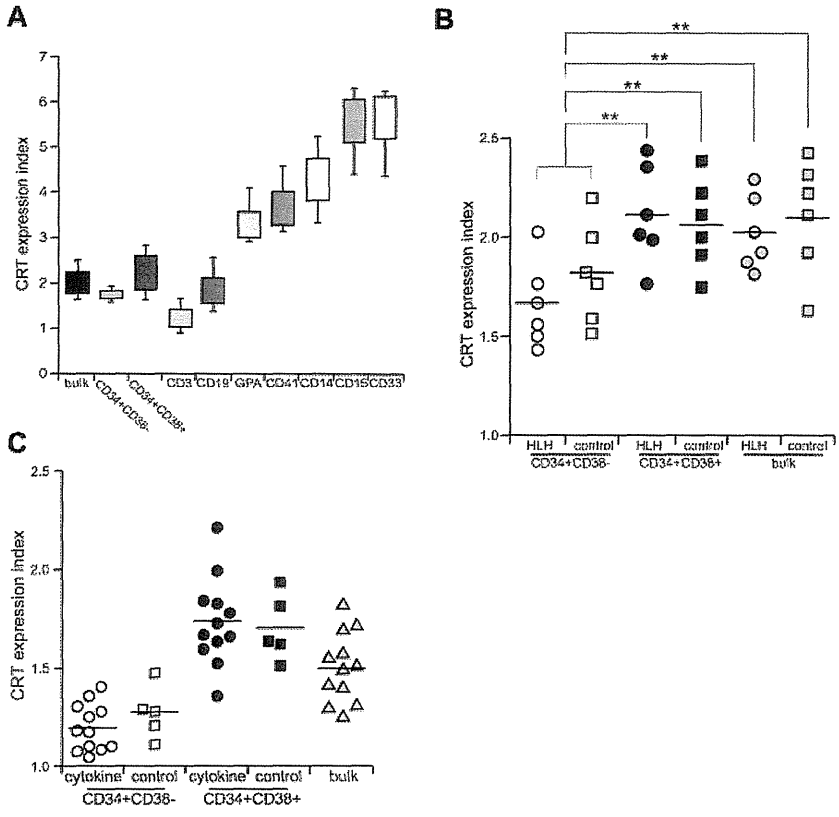

Figure 6. CRT is not involved in the engulfment of HSCs in HLH. (A) CRT expression in normal hematopoietic cells. CRT expression index represents the relative surface CRT level calculated as median CRT levels of analyzed cells/those in normal blood mononuclear cells. Error bars show 1 SD differences. (B) CRT expression in $CD34^+CD38^-$ HSCs, $CD34^+CD38^+$ progenitors, and unfractionated BM cells from HLH patients and healthy controls. The expression level of CRT was equivalent in HLH patients and healthy controls in all of these cell fractions. $^{**}P < .05$ by conventional *t* test. (C) The effect of cytokines on CRT expression. CRT expression was not changed irrespective of incubation with cytokines in any of these cell fractions. Bars show the mean values.

$CD34^+CD38^-$ cells occurs in response to cytokines in a dose-dependent manner (Figure 5C). The cells treated with cytokines were further tested for phagocytosis assays. As shown in Figure 5D, the expression level of CD47 in $CD34^+CD38^-$ HSCs treated with inflammatory cytokines was inversely correlated with the phagocytosis index. These data suggest that inflammatory cytokines can down-regulate CD47 expression specifically in HSCs, inducing HSC-targeted engulfment by BM macrophages.

CRT, a dominant prophagocytic factor, is down-regulated in $CD34^+CD38^-$ HSCs in both HLH patients and healthy controls

CRT is the major prophagocytic factor expressed on the cell surface, which binds to lipoprotein-related protein on cell surface of macrophages and stimulates their phagocytic activities.[14] During apoptotic cell death, these cells are engulfed due to loss of CD47 expression and coordinated up-regulation of cell-surface CRT as thedominant prophagocytic signal.[38] We evaluated the expression level of CRT in stem, progenitor, and mature cell fractions in HLH patients. In the healthy BM, CRT was highly expressed in mature myeloid cells, but at a very low level in lymphoid cells. Erythroblasts and megakaryocytes expressed intermediate levels of CRT. Interestingly, the expression level of CRT was very low in immature hematopoietic cells, including $CD34^+CD38^-$ HSCs and $CD34^+CD38^+$ progenitor cell fractions (Figure 6A). $CD34^+CD38^-$ HSCs expressed even lower levels of CRT compared with those in $CD34^+CD38^+$ progenitors (Figure 6B). In HLH patients, the expression of CRT was comparable to that in healthy controls: The $CD34^+CD38^-$ HSC population expressed only a very low level of CRT (Figure 6B). We then cultured normal HSCs in the presence of inflammatory cytokines including M-CSF, IL-6, IFN-γ, and TNF-α for 24 hours, and the expression of CRT did not change in the HSC or progenitor populations (Figure 6C). Therefore, CRT is shut down at the HSC stage even in HLH patients, suggesting that the expression of CRT is not involved in engulfment of HSCs by macrophages.

Discussion

In HLH, cytopenia occurs in more than 80% of patients at disease presentation. The BM may present either hypocellularity or hypercellularity at the onset, but eventually becomes hypoplastic. This phenotype is thought to result mainly from suppression of hematopoiesis by elevated inflammatory cytokines such as TNF-α and IFN-γ and from engulfment of hematopoietic cells by BM macrophages.[39] The serum concentrations of these cytokine levels in HLH are usually quite higher than those with sepsis,[40] suggesting that these extremely high levels of cytokines should be critical in the pathogenesis of HLH. In the present study, we show that HLH patients have low numbers of HSCs, and that HSCs from HLH patients down-regulate CD47 and are prone to be engulfed by macrophages more actively than normal HSCs. We also show that inflammatory cytokines can down-regulate the expression of CD47 selectively in HSCs, resulting in a disruption of self-recognition based on the CD47-SIRPA system to induce engulfment of HSCs by macrophages. Based on these data, we propose that the disruption of the CD47-SIRPA system plays a primary role in the development of HLH.

Macrophages function to clear foreign, aged, or damaged cells via phagocytosis, and this process is regulated by the balance between antiphagocytic and prophagocytic signals. The primary

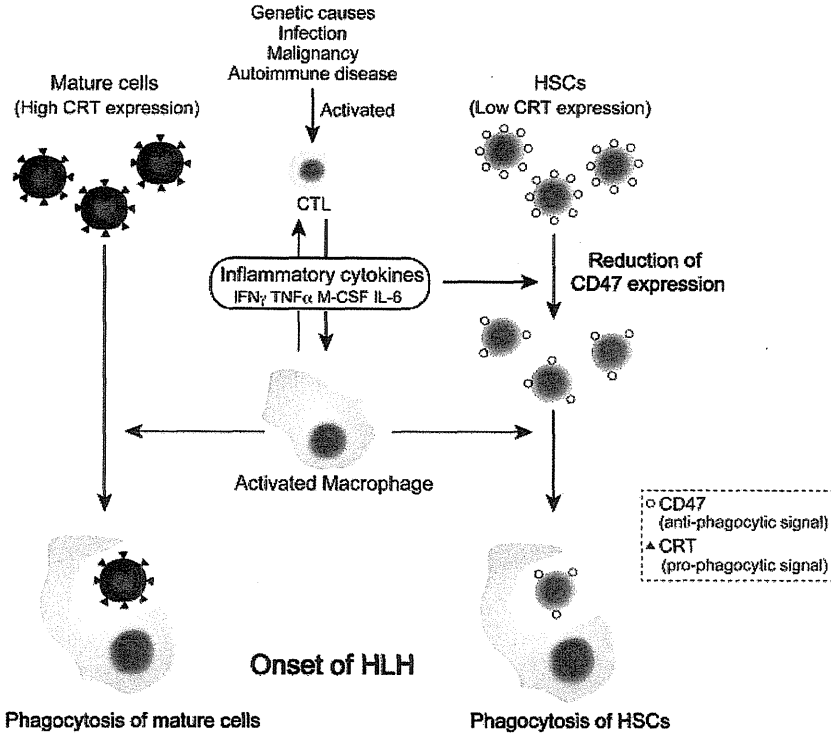

Figure 7. Pathogenesis of HLH based on antiphagocytic and prophagocytic signaling. In HLH, cytotoxic T lymphocytes are activated by genetic abnormality, infection, malignancy, and autoimmune disease, and then produce inflammatory cytokines and activate macrophages. Activated macrophages engulf mature cells such as RBCs, platelets, and granulocytes, which are susceptible to phagocytosis because of high expression of prophagocytic CRT. In contrast, inflammatory cytokines suppress hematopoiesis by their direct toxic effects and down-regulate CD47 expression on HSCs, resulting in a decreased threshold of antiphagocytic signals. Therefore, HSCs were engulfed by activated macrophages, causing the BM of HLH patients to become hypoplastic, thereby exacerbating pancytopenia.

antiphagocytic and prophagocytic signals for macrophages to engulf nonapoptotic cells are the CD47-SIRPA and the LPR-CRT systems, respectively.[14] Because in the present study, freshly isolated HSCs from HLH patients, but not from healthy controls, were engulfed by macrophages in vitro (Figure 4A), the balancing of this signaling should be altered in HLH.

Many polymorphisms have been detected in human SIRPA, especially in the ligand-binding IgV domain.[26] In the present study, however, HLH patients did not have any specific polymorphisms of SIRPA. In addition, we could not find differences in the level of SIRPA expression between normal and HLH BM cells. We conclude that neither polymorphisms of SIRPA nor the change of its expression levels are involved in the pathogenesis of HLH.

Conversely, the expression of CD47 was significantly down-regulated specifically in the HSC fraction in HLH patients, but was not changed in progenitors and other mature cells (Figure 2A-C). The expression level of CD47 in HLH HSCs was approximately 50% at the protein level compared with that in normal HSCs. This level of reduction readily induced macrophage activation in vitro (supplemental Figures 2 and 4A). BM HSCs in HLH patients were reduced in number, presumably by engulfment, but were functionally normal, at least in terms of colony-forming capabilities in vitro (supplemental Figure 1B). The down-regulation of CD47 in HLH HSCs might be induced by high levels of serum inflammatory cytokines such as IL-6, M-CSF, IFN-γ, and TNF-α, because incubation of normal HSCs, but not progenitors, with these cytokines induced down-regulation of CD47 in vitro in a dose-dependent manner (Figure 5B-C), and rendered normal HSCs susceptible to engulfment by macrophages (Figure 5D).

It remains unclear by what mechanism only the HSC fraction is sensitive to cytokines to down-regulate CD47. Interestingly, in contrast to the CD47 protein, the CD47 mRNA levels were normal in HSCs in all 5 HLH patients analyzed by quantitative real-time PCR assays (not shown), so the down-regulation of CD47 could occur at the posttranscriptional level. In a recent study, Junker et al examined miRNA profiles from active and inactive lesions in multiple sclerosis patients, and found out that miRNA-34a, miRNA-155 and miRNA-326, the targets of which include human CD47, were up-regulated in active sclerosis lesions.[41] These miRNAs reduce the expression of CD47 in brain-resident cells, promoting macrophages to engulf myelin. In the present study, we evaluated miRNA-34a, miRNA-155, and miRNA-326 expression in HSCs in HLH patients, but could not find any differences in the expression level of these miRNAs in HSCs from HLH patients and healthy controls (T.K., unpublished data, February 2010). Inflammatory cytokines did not induce the increased expression of these miRNAs (T.K., unpublished data, March 2010). It is critical to clarify the mechanism of CD47 down-regulation in the HSC fraction in future studies.

The expression of CRT on the cell surface is an important prophagocytic signal. When CRT binds to LPR on macrophages, LPR signaling immediately can stimulate macrophages to engulf the CRT-expressing cells.[14,15] This "eat me" signal could antagonize the "do not eat me" signal mediated by the CD47-SIRPA interaction.[42] Once apoptosis is initiated, CRT is up-regulated, phosphatidylserine is exposed to the cell surface, and CD47-SIRPA signaling is rendered ineffective, thereby permitting engulfment of target cells.[42] In contrast to CD47, which is ubiquitously expressed in normal hematopoietic cells from HSCs to mature cell stages (Figure 2A), CRT is expressed mainly in myeloerythroid cells, but only at a low level in immature $CD34^+CD38^-$ HSCs. Because recent studies have shown that macrophages are cellular components of HSC niches,[24] down-regulation of CRT might be required for HSCs to stay intact at the niche. In contrast, mature myeloerythroid cells might be primed to be prophagocytic via sustained CRT expression, which enables macrophages to engulf these cells on activation by, for example, cytokines.

Previous studies have shown that the CD47-SIRPA system is critical to engraftment and maintenance of HSCs in vivo. We have reported that the reason that human HSCs engraft efficiently in the

NOD mouse is that this strain has a polymorphic SIRPA capable of binding to human CD47.[26] Blocking the CD47-SIRPA interaction by antihuman CD47 Fc inhibited the engraftment of human HSCs in the NOD-SCID xenograft model. In fact, HSCs have contact with macrophages in the vascular or reticuloendothelial niche,[43,44] suggesting that self-recognition by macrophages could operate actively at the HSC niche. The impairment of antiphagocytic signals that involves HSCs specifically may be one of the primary mechanisms for the severe hypocellularity and pancytopenia seen in the BM of HLH patients.

A schematic of the proposed pathogenesis of HLH based on the results of the present study is provided in Figure 7. In HLH, elevated inflammatory cytokines activate macrophages. Mature blood cells with high levels of CRT expression might be readily ingested by macrophages on activation compared with immature cells. The prophagocytic CRT is not expressed in HSCs; however, HSCs cannot compensate for the loss of mature cells in HLH by enhancement of hematopoiesis, because HSCs are also targeted by BM macrophages through inhibition of surface CD47 expression by inflammatory cytokines. The down-regulation of CD47 in HSCs abrogates the antiphagocytic SIRPA signal, resulting in active engulfment of HSCs by macrophages, presumably at the HSC niche. Therefore, hemophagocytosis in HLH occurs by at least 2 independent pathways mediated by CRT or CD47.

We have reported previously that in HLH patients, activated macrophages and monocytes produce a high level of cytokines such as IL-6 and TNF-α, whereas activated T cells produce IFN-γ and M-CSF.[3] These cytokines may cause the down-regulation of CD47 in HSCs that further activate macrophages. Therefore, to trigger HLH development, activation of both acquired and innate immune systems might be required. Nonetheless, our present data highlight the importance of CD47-SIRPA axis in the development of HLH, by which the HSC, the source of all blood cells, becomes the target for engulfment. Accordingly, our results suggest that the CD47-Fc protein that can bind to SIRPA on activated macrophages may be able to suppress the deregulated engulfment of HSCs in HLH. Understanding the mechanism of HSC-specific down-regulation of CD47 will be critical to the development of future therapeutic approaches for HLH.

Acknowledgments

The authors thank the Kyushu Block Red Cross Blood Center for providing umbilical cord blood samples.

This work was supported in part by a grant-in-aid from the Ministry of Education, Culture, Sports, Science and Technology in Japan (to K.A. and K.T.); a grant-in-aid from the Ministry of Health, Labor and Welfare in Japan (to K.A.); the Takeda Science Foundation (to K.T.); and the Cell Science Research Foundation (to K.T.).

Authorship

Contribution: T.K. and K.T. coordinated the project, designed and performed the experiments, analyzed the data, and wrote the manuscript; K.K., T.Y., S.D., G.Y., and Y.K. performed the experiments; J.K. analyzed the data; Y.A. and N.H. provided technical advice; and T.M., H.I., T.T., and K.A. designed the experiments, reviewed the data, and edited the manuscript.

Conflict-of-interest disclosure: The authors declare no competing financial interests.

Correspondence: Katsuto Takenaka, MD, PhD, Department of Medicine and Biosystemic Science, Kyushu University Graduate School of Medical Sciences, 3-1-1 Maidashi, Higashi-ku, Fukuoka 812-8582, Japan; e-mail: takenaka@intmed1.med.kyushu-u.ac.jp.

References

1. Janka GE. Familial and acquired hemophagocytic lymphohistiocytosis. *Eur J Pediatr.* 2007; 166(2):95-109.
2. Filipovich A, McClain K, Grom A. Histiocytic disorders: recent insights into pathophysiology and practical guidelines. *Biol Blood Marrow Transplant.* 2010;16(1 Suppl):S82-89.
3. Akashi K, Hayashi S, Gondo H, et al. Involvement of interferon-gamma and macrophage colony-stimulating factor in pathogenesis of haemophagocytic lymphohistiocytosis in adults. *Br J Haematol.* 1994;87(2):243-250.
4. Ishii E, Ohga S, Imashuku S, et al. Nationwide survey of hemophagocytic lymphohistiocytosis in Japan. *Int J Hematol.* 2007;86(1):58-65.
5. Stepp SE, Dufourcq-Lagelouse R, Le Deist F, et al. Perforin gene defects in familial hemophagocytic lymphohistiocytosis. *Science.* 1999;286(5446):1957-1959.
6. Feldmann J, Callebaut I, Raposo G, et al. Munc13-4 is essential for cytolytic granules fusion and is mutated in a form of familial hemophagocytic lymphohistiocytosis (FHL3). *Cell.* 2003; 115(4):461-473.
7. zur Stadt U, Schmidt S, Kasper B, et al. Linkage of familial hemophagocytic lymphohistiocytosis (FHL) type-4 to chromosome 6q24 and identification of mutations in syntaxin 11. *Hum Mol Genet.* 2005;14(6):827-834.
8. zur Stadt U, Rohr J, Seifert W, et al. Familial hemophagocytic lymphohistiocytosis type 5 (FHL-5) is caused by mutations in Munc18-2 and impaired binding to syntaxin 11. *Am J Hum Genet.* 2009; 85(4):482-492.
9. Bizario JC, Feldmann J, Castro FA, et al. Griscelli syndrome: characterization of a new mutation and rescue of T-cytotoxic activity by retroviral transfer of RAB27A gene. *J Clin Immunol.* 2004; 24(4):397-410.
10. Underhill DM, Ozinsky A. Phagocytosis of microbes: complexity in action. *Annu Rev Immunol.* 2002;20:825-852.
11. Greaves DR, Gordon S. Thematic review series: the immune system and atherogenesis. Recent insights into the biology of macrophage scavenger receptors. *J Lipid Res.* 2005;46(1):11-20.
12. McGreal EP, Martinez-Pomares L, Gordon S. Divergent roles for C-type lectins expressed by cells of the innate immune system. *Mol Immunol.* 2004;41(11):1109-1121.
13. Miyanishi M, Tada K, Koike M, Uchiyama Y, Kitamura T, Nagata S. Identification of Tim4 as a phosphatidylserine receptor. *Nature.* 2007; 450(7168):435-439.
14. Gardai SJ, McPhillips KA, Frasch SC, et al. Cell-surface calreticulin initiates clearance of viable or apoptotic cells through trans-activation of LRP on the phagocyte. *Cell.* 2005;123(2):321-334.
15. Orr AW, Pedraza CE, Pallero MA, et al. Low density lipoprotein receptor-related protein is a calreticulin coreceptor that signals focal adhesion disassembly. *J Cell Biol.* 2003;161(6):1179-1189.
16. Fadok VA, Bratton DL, Henson PM. Phagocyte receptors for apoptotic cells: recognition, uptake, and consequences. *J Clin Invest.* 2001;108(7): 957-962.
17. Brown EJ, Frazier WA. Integrin-associated protein (CD47) and its ligands. *Trends Cell Biol.* 2001;11(3):130-135.
18. Matozaki T, Murata Y, Okazawa H, Ohnishi H. Functions and molecular mechanisms of the CD47-SIRPalpha signalling pathway. *Trends Cell Biol.* 2009;19(2):72-80.
19. van den Berg TK, van der Schoot CE. Innate immune 'self' recognition: a role for CD47-SIRPalpha interactions in hematopoietic stem cell transplantation. *Trends Immunol.* 2008;29(5):203-206.
20. Adams S, van der Laan LJ, Vernon-Wilson E, et al. Signal-regulatory protein is selectively expressed by myeloid and neuronal cells. *J Immunol.* 1998;161(4):1853-1859.
21. Barclay AN. Signal regulatory protein alpha (SIRPalpha)/CD47 interaction and function. *Curr Opin Immunol.* 2009;21(1):47-52.
22. Oldenborg PA, Zheleznyak A, Fang YF, Lagenaur CF, Gresham HD, Lindberg FP. Role of CD47 as a marker of self on red blood cells. *Science.* 2000; 288(5473):2051-2054.
23. Blazar BR, Lindberg FP, Ingulli E, et al. CD47 (integrin-associated protein) engagement of dendritic cell and macrophage counterreceptors is required to prevent the clearance of donor lymphohematopoietic cells. *J Exp Med.* 2001;194(4): 541-549.
24. Winkler IG, Sims NA, Pettit AR, et al. Bone marrow macrophages maintain hematopoietic stem cell (HSC) niches and their depletion mobilizes HSCs. *Blood.* 2010;116(23):4815-4828.
25. Ehninger A, Trumpp A. The bone marrow stem cell niche grows up: mesenchymal stem cells and

macrophages move in. *J Exp Med.* 2011;208(3):421-428.

26. Takenaka K, Prasolava TK, Wang JC, et al. Polymorphism in Sirpa modulates engraftment of human hematopoietic stem cells. *Nat Immunol.* 2007;8(12):1313-1323.
27. Henter JI, Horne A, Arico M, et al. HLH-2004: diagnostic and therapeutic guidelines for hemophagocytic lymphohistiocytosis. *Pediatr Blood Cancer.* 2007;48(2):124-131.
28. Tsuda H. Hemophagocytic syndrome (HPS) in children and adults. *Int J Hematol.* 1997;65(3):215-226.
29. Manz MG, Miyamoto T, Akashi K, Weissman IL. Prospective isolation of human clonogenic common myeloid progenitors. *Proc Natl Acad Sci U S A.* 2002;99(18):11872-11877.
30. Mori Y, Iwasaki H, Kohno K, et al. Identification of the human eosinophil lineage-committed progenitor: revision of phenotypic definition of the human common myeloid progenitor. *J Exp Med.* 2009;206(1):183-193.
31. Fujimi A, Matsunaga T, Kobune M, et al. Ex vivo large-scale generation of human red blood cells from cord blood CD34+ cells by coculturing with macrophages. *Int J Hematol.* 2008;87(4):339-350.
32. Hashimoto S, Yamada M, Motoyoshi K, Akagawa KS. Enhancement of macrophage colony-stimulating factor-induced growth and differentiation of human monocytes by interleukin-10. *Blood.* 1997;89(1):315-321.
33. Jaiswal S, Jamieson CH, Pang WW, et al. CD47 is upregulated on circulating hematopoietic stem cells and leukemia cells to avoid phagocytosis. *Cell.* 2009;138(2):271-285.
34. Barclay AN, Hatherley D. The counterbalance theory for evolution and function of paired receptors. *Immunity.* 2008;29(5):675-678.
35. Majeti R, Chao MP, Alizadeh AA, et al. CD47 is an adverse prognostic factor and therapeutic antibody target on human acute myeloid leukemia stem cells. *Cell.* 2009;138(2):286-299.
36. Nagafuji K, Nonami A, Kumano T, et al. Perforin gene mutations in adult-onset hemophagocytic lymphohistiocytosis. *Haematologica.* 2007;92(7):978-981.
37. Chao MP, Alizadeh AA, Tang C, et al. Anti-CD47 antibody synergizes with rituximab to promote phagocytosis and eradicate non-Hodgkin lymphoma. *Cell.* 2010;142(5):699-713.
38. Chao MP, Jaiswal S, Weissman-Tsukamoto R, et al. Calreticulin is the dominant pro-phagocytic signal on multiple human cancers and is counterbalanced by CD47. *Sci Transl Med.* 2010;2(63):63ra94.
39. Maciejewski J, Selleri C, Anderson S, Young NS. Fas antigen expression on CD34+ human marrow cells is induced by interferon gamma and tumor necrosis factor alpha and potentiates cytokine-mediated hematopoietic suppression in vitro. *Blood.* 1995;85(11):3183-3190.
40. Wu HP, Chen CK, Chung K, et al. Serial cytokine levels in patients with severe sepsis. *Inflamm Res.* 2009;58(7):385-393.
41. Junker A, Krumbholz M, Eisele S, et al. MicroRNA profiling of multiple sclerosis lesions identifies modulators of the regulatory protein CD47. *Brain.* 2009;132(Pt 12):3342-3352.
42. Martins I, Kepp O, Galluzzi L, et al. Surface-exposed calreticulin in the interaction between dying cells and phagocytes. *Ann N Y Acad Sci.* 2010;1209:77-82.
43. Nagasawa T, Omatsu Y, Sugiyama T. Control of hematopoietic stem cells by the bone marrow stromal niche: the role of reticular cells. *Trends Immunol.* 2011;32(7):315-320.
44. Morrison SJ, Spradling AC. Stem cells and niches: mechanisms that promote stem cell maintenance throughout life. *Cell.* 2008;132(4):598-611.

Graft-versus-host disease disrupts intestinal microbial ecology by inhibiting Paneth cell production of α-defensins

Yoshihiro Eriguchi,[1] Shuichiro Takashima,[1] Hideyo Oka,[1] Sonoko Shimoji,[1] Kiminori Nakamura,[2] Hidetaka Uryu,[1] Shinji Shimoda,[1] Hiromi Iwasaki,[3] Nobuyuki Shimono,[1] Tokiyoshi Ayabe,[2] Koichi Akashi,[1,3] and Takanori Teshima[3]

[1]Department of Medicine and Biosystemic Science, Kyushu University Graduate School of Medical Science, Fukuoka, Japan; [2]Department of Cell Biological Science, Graduate School of Life Science, Faculty of Advanced Life Science, Hokkaido University, Sapporo, Japan; and [3]Center for Cellular and Molecular Medicine, Kyushu University Graduate School of Medical Science, Fukuoka, Japan

Allogeneic hematopoietic stem cell transplantation (SCT) is a curative therapy for various hematologic disorders. Graft-versus-host disease (GVHD) and infections are the major complications of SCT, and their close relationship has been suggested. In this study, we evaluated a link between 2 complications in mouse models. The intestinal microbial communities are actively regulated by Paneth cells through their secretion of antimicrobial peptides, α-defensins. We discovered that Paneth cells are targeted by GVHD, resulting in marked reduction in the expression of α-defensins, which selectively kill noncommensals, while preserving commensals. Molecular profiling of intestinal microbial communities showed loss of physiologic diversity among the microflora and the overwhelming expansion of otherwise rare bacteria *Escherichia coli*, which caused septicemia. These changes occurred only in mice with GVHD, independently on conditioning-induced intestinal injury, and there was a significant correlation between alteration in the intestinal microbiota and GVHD severity. Oral administration of polymyxin B inhibited outgrowth of *E coli* and ameliorated GVHD. These results reveal the novel mechanism responsible for shift in the gut flora from commensals toward the widespread prevalence of pathogens and the previously unrecognized association between GVHD and infection after allogeneic SCT. (*Blood*. 2012;120(1): 223-231)

Introduction

Allogeneic hematopoietic stem cell transplantation (SCT) is a curative therapy for hematologic malignant tumors, bone marrow failure, and congenital metabolic disorders. Graft-versus-host disease (GVHD) and related infections are major obstacles to SCT, and their close relationship has been indicated in clinical settings. Septicemia is the most life-threatening infection after allogeneic SCT and gram-negative rods are the most dominant pathogens of septicemia, whereas incidence of drug-resistant enterococci infection increase in neutropenic patients colonized with these bacteria in some centers.[1] GVHD is one of the major predisposing factors for the development of septicemia.[2] Since the pioneering works of van Bekkum[3] and others in the 1960s-1970s, interaction between intestinal flora and GVHD has been suggested.[3-6]

We recently demonstrated that intestinal stem cells (ISCs), which are essential to repair damaged intestinal epithelium, are targeted by GVHD.[7] Recently, Paneth cells located besides ISCs within the crypts are identified as niche for ISCs.[8] In addition, Paneth cells are essential regulators of the composition of intestinal microbiota by secreting antimicrobial peptides, α-defensins, which provide broad-spectrum antimicrobial properties by pore formation in the bacterial cell walls.[9-11] The intestine, which is the major interface between the environment and the host, is an open ecologic system that is colonized by at least 1000 distinct bacterial species, of which more than 80% are nonculturable.[12-14] Accurate identification of species in the gut microbiota requires culture-independent, molecular profiling methods. Firmicutes and Bacteroidetes make up approximately 90% of the intestinal microbiota.[12,15] These commensals are rarely pathogenic and instead make several essential contributions to human physiology and health.[12,13,15,16] In contrast, Gammaproteobacteria such as *Escherichia coli*, which have a gram-negative cell wall make up a small proportion of the microbiota.[17] A recent study showed an increase in gram-negative *Enterobacteriaceae* family members including *E coli* among the intestinal microbiota after allogeneic bone marrow transplantation (BMT) in mice.[18] It remains unclear why they are most frequent pathogens in patients with intestinal GVHD, although the role of systemic immunosuppression and use of antibiotics has been well appreciated.[19]

In this study, we focused on Paneth cells and evaluated the possible mechanistic links between GVHD and infection in mouse models of BMT. We found that GVHD targets Paneth cells and causes subsequent impairment of antimicrobial peptide secretion, leading to marked loss of diversity among the intestinal microflora. This results in shift in the gut flora from commensal microorganisms toward the widespread prevalence of gram-negative bacteria and development of bloodstream infection.

Methods

Mice

Female C57BL/6 (B6: H-2^b), B6D2F1 (H-2$^{b/d}$), B6C3F1 (H-2$^{b/k}$), B6-Ly5.1 (H-2^b, CD45.1$^+$), and C3H.Sw (H-2^b) mice were purchased from Charles

Submitted December 25, 2011; accepted April 22, 2012. Prepublished online as *Blood* First Edition paper, April 24, 2012; DOI 10.1182/blood-2011-12-401166.

There is an Inside *Blood* commentary on this article in this issue.

The publication costs of this article were defrayed in part by page charge payment. Therefore, and solely to indicate this fact, this article is hereby marked "advertisement" in accordance with 18 USC section 1734.

River Japan, KBT Oriental, or Japan SLC. All animal experiments were performed under the auspices of the Institutional Animal Care and Research Advisory Committee.

BMT

Mice were transplanted as previously described.[20] In brief, after lethal x-ray total body irradiation (TBI) delivered in 2 doses at 4-hour intervals, mice were intravenously injected with 5×10^6 T-cell depleted bone marrow (TCD-BM) cells with or without 2×10^6 splenic T cells on day 0. Isolation of T cells and T-cell depletion were performed using the T-cell isolation kit and anti-CD90 microBeads, respectively, and the AutoMACS (Miltenyi Biotec) according to the manufacturer's instructions. In some experiments, unirradiated B6D2F1 mice were intravenously injected with 12×10^7 splenocytes.[7] Mice were maintained in specific pathogen-free conditions and received normal chow and autoclaved hyperchlorinated water (Ph 4) for the first 3 weeks after BMT and filtered water thereafter. Polymyxin B (Calbiochem) diluted in water was administered by daily oral gavage at a dose of 100 mg/kg from day −4 until day 28 after BMT. Survival after BMT was monitored daily and the degree of clinical GVHD was assessed weekly by a scoring system which sums changes in 5 clinical parameters: weight loss, posture, activity, fur texture, and skin integrity (maximum index = 10) as previously described.[20]

Histologic and immunohistochemical analysis

For pathologic analysis, samples of the small intestine were fixed in 10% neutral-buffered formalin, embedded in paraffin, sectioned, slide mounted, and stained with H&E. Immunohistochemistry was performed as described[21] using rabbit anti-lysozyme (Dako) and rabbit anti-defensin1. Histofine simple stain MAX PO (Rat) kits and subsequently diaminobenzide (DAB) solution (Nichirei Biosciences) was used to generate brown-colored signals. Slides were then counterstained with hematoxylin. Pictures from tissue sections were taken at room temperature using a digital camera (DP72; Olympus) mounted on a microscope (BX51; Olympus). Acute GVHD was assessed by detailed histopathologic analysis using a semiquantitative scoring system.[22]

Preparation and analysis of isolated mouse crypts

Individual crypts were isolated from the small intestine as previously described.[23] Isolated crypts were fixed with 2% paraformaldehyde in PBS for 20 minutes and permeabilized with 0.2% Triton X-100 in PBS for 5 minutes. Crypts were incubated for 1 hour with fluorescein isothiocyanate-conjugated anti-lysozyme (10 μg/mL; Dako), washed 3 times in PBS, followed by incubation for 1 hour with Allexa Fluor 594–conjugated phalloidin (1 U/mL; Invitrogen). Tetramethyl 4,6-diamidino-2-phenylindole (DAPI; 5 μg/mL; Invitrogen) was used to stain the nucleus. Samples were mounted in aqua poly/mount (Polysciences) and examined with a confocal laser-scanning microscope (LSM510; Carl Zeiss).

Enzyme-linked immunosorbent assay

The limulus amebocyte lysate assay QCL-1000 (Lonza) was performed according to the manufacturer's instructions to determine the serum level of lipopolysaccharide (LPS) with a sensitivity of 0.1 EU/mL. All units expressed are relative to the United States reference standard EC-2.

Quantitative real-time PCR analysis

Total RNA was purified using the RNeasy Kit (QIAGEN). cDNA was synthesized using a QuantiTect reverse transcription kit (QIAGEN). Polymerase chain reactions (PCRs) and analyses were performed with ABI PRISM 7900HT SDS 2.1 (Applied Biosystems) using TaqMan universal PCR master mix (Applied Biosystems), and TaqMan gene expression assays (Defa1: Mm02524428_g1, Defa4: Mm00651736_g1, Defa5: Mm00651548_g1, Defa21/Defa22: Mm04206099_gH, Defcr-rs1: Mm00655850_m1, Lyz1: Mm00657323_m1, and Gapdh: Mm99999915_g1; Applied Biosystems). The relative amount of each mRNA was determined using the standard curve method and was normalized to the level of GAPDH in each sample.

Total fecal bacterial DNA extraction

Total DNA was isolated from fecal pellets using a QIAamp DNA stool mini kit (QIAGEN) with bead beating treatment during the cell-lysis step. Briefly, fresh fecal pellets were collected from individual mice; 0.5 g baked 0.1 mm zirconia/silica beads (Biospec Products) and ASL buffer were added to each aliquot. Fecal samples with ASL buffer were incubated at 95°C, and samples were processed for 1 minute at speed 5.5 on Fastprep system (Qbiogene).[24]

PCR amplification of 16S rRNA gene

Bacterial 16S ribosomal RNA (rRNA) genes were amplified with bacterial-universal primers, 27F (5′-AGAGTTTGATCCTGGCTCAG-3′) labeled at the 5′ end with 6-carboxyfluorescein (6-FAM) and 1492R (5′-GGTTACCTTGT TACGACTT-3′).[25] PCR amplification was performed using *EX Taq* (Takara Bio) and the following program: 3 minutes of denaturation at 95°C, 30 cycles of 0.5 minute at 95°C, 0.5 minute at 50°C, 1.5 minute at 72°C, and a final 10 minutes extension step at 72°C in a BiometraT3 thermocycler (Biometra). Amplicons were purified using a QIAquick PCR Purification kit (QIAGEN).

Restriction fragment length polymorphism (RFLP) analysis

The purified DNA products (3 μL) were digested with 10 U of either *Hha*I or *Msp*I (Takara Bio) in a total volume of 10 μL at 37°C for 3 hours. The restriction digest products (2 μL) were mixed with 10 μL deionized formamide and 0.5 μL GeneScan-1200 LIZ standard (Applied Biosystems). The samples were denatured at 95°C for 2 minutes, followed by rapid chilling on ice. The fluorescently labeled fragments (T-RFs) were separated by size on an ABI 3130 genetic analyzer (Applied Biosystems). The electropherograms were analyzed with GeneMapper Version 4.0 software (Applied Biosystems), and the fragment sizes were estimated using the Local Southern method. Each unique RFLP pattern was designated as an operational taxonomic unit (OTU). OTUs with a peak area of less than 0.5% of the total area were excluded from the analysis. Proportion of *E coli* was defined as the ratio of area of OTU for *E coli* to total areas of OTUs. Diversity of the microbial community corresponding to the RFLP banding pattern was calculated using the Simpson index of diversity 1-D ($D = \Sigma pi^2$)[26] and Shannon diversity index H′ ($H' = -\Sigma piln(pi)$)[27] and where pi is the proportion of total number of species made up of its species.

Cloning and sequencing analysis

Internal region of the 16S rRNA genes were amplified using 27F and 806R (5′-GGACTACCAGGGTATCTAAT-3′) primers, and were transformed using TOPO TA Cloning Kit with TOP10 *E coli* (Invitrogen). The nucleotide sequences of inserts were determined using the M13 forward and reverse primers. All sequences were examined for possible chimeric artifacts by the Chimera check with Bellerophon Version 3. After eliminating chimeric sequences, the partial 16S rRNA sequences were compared with the sequences in the Ribosomal Database Project and GenBank, using the BLAST program (http://www.ncbi.nlm.nih.gov/BLAST/). Cloned sequences were identified as representing the species or phylotype of the sequence with the highest matching score. Sequences with less than 98% identity with a GenBank sequence were defined as a new phylotype. In addition, we checked whether the sequenced clones had the correct T-RFs compared with the sequence information.

Microbiologic analysis of bacterial translocation

The livers and mesenteric lymph nodes (mLNs) isolated from mice that had received transplants were removed aseptically and homogenized in 1 mL saline. Then, 500 μL of homogenate was transferred into a tube containing 4.5 mL of saline and used to perform 4 serial dilutions. From this dilution, 100 μL aliquots were cultured aerobically on blood agar and LB agar plates (Difco) for 24 hours at 37°C in room air supplemented with 10% CO_2. Colony-forming units (CFUs) were counted and adjusted per organ. Bacteria were identified by biochemical profiles.

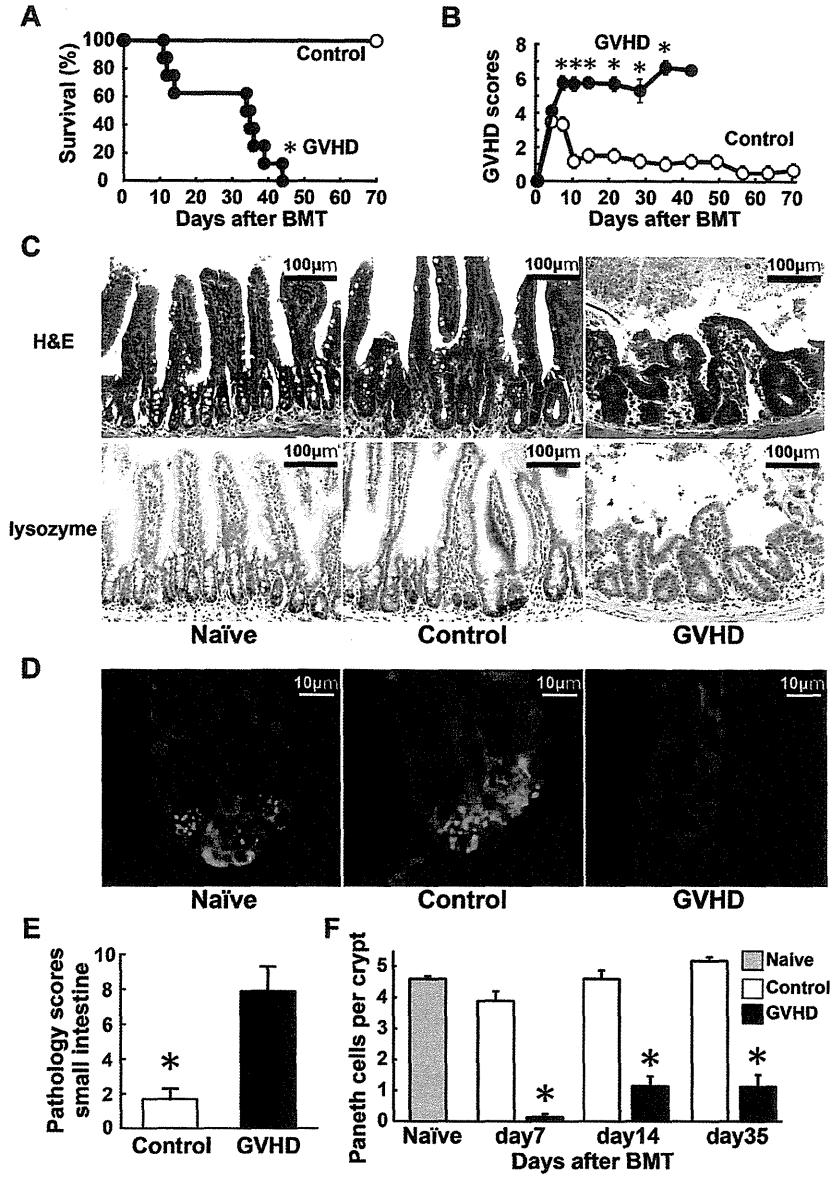

Figure 1. Paneth cell injury in GVHD. Lethally irradiated B6D2F1 mice were transplanted with 5×10^6 TCD BM cells without (control group, n = 6) or with 2×10^6 T cells (GVHD group, n = 12) from MHC-mismatched B6 donors on day 0. (A-B) Survival (A) and clinical GVHD scores (B) means ± SE are shown. Data from 2 independent experiments were combined. (C-F) Small intestines were isolated from mice 7 days after BMT. (C) Top panels: histology of the small intestine stained with H&E. Bottom panels: Lysozyme staining (brown). Magnification:100×. Bars, 100 μm. (D) Confocal cross-sectioning of the isolated small intestinal crypt. Lysozyme (green) is expressed by Paneth cells. Tetramethyl DAPI (blue) stains the nucleus and phalloidin (red) stains F-actin. Magnification: 1000×. Bars, 10 μm. (E) Pathology scores of the small intestine (mean ± SE, n = 3-6 / group). (F) Quantification of Paneth cells per crypt (mean ± SE, n = 3-6 / group; $^*P < .05$).

Statistical analysis

Mann-Whitney *U* tests were used to compare data, the Kaplan-Meier product limit method was used to obtain survival probability, and the log-rank test was applied to compare survival curves. To determine the statistically significant correlation, the Spearman rank correlation coefficient (R) was adopted. All tests were performed with SigmaPlot Version 10.0 software. $P < .05$ was considered statistically significant.

Accession numbers

Sequence data are available in the GenBank (http://www.ncbi.nih.gov/genbank) under the accession number 1509996.

Results

Paneth cell damage and decreased expression of α-defensins in GVHD

We evaluated whether Paneth cells could be damaged during GVHD. Lethally irradiated B6D2F1 (H-$2^{b/d}$) mice received 5×10^6 TCD-BM cells (control group) or these cells plus 2×10^6 T cells (GVHD group) from major histocompatibility complex (MHC)–mismatched B6 (H-2^b) donors on day 0. The allogeneic animals developed severe GVHD and all of these mice died within 50 days after BMT, whereas all TCD-BM controls survived through this period (Figure 1A). The surviving allogeneic animals showed significantly more severe signs of GVHD than controls, as assessed by clinical GVHD scores[20] (Figure 1B). Pathologic analysis of the small intestine 7 days after BMT showed mostly normal architecture in controls, whereas severe blunting of villi and inflammatory infiltration were observed in the GVHD group (Figure 1C). Paneth cells, which are typically identified microscopically by their location in the crypts and by the large granules occupying most of their cytoplasm, were hardly observed in the GVHD group. Immunohistochemical analysis for lysozyme, which indicates the presence of Paneth cells, confirmed loss of Paneth cells in the GVHD group, but not in controls (Figure 1C). Confocal cross-sectioning of individual crypts isolated from the small intestine further confirmed Paneth cell loss in these mice (Figure 1D). In mice with GVHD, GVHD pathology scores were significantly higher (Figure 1E), whereas numbers of Paneth cells

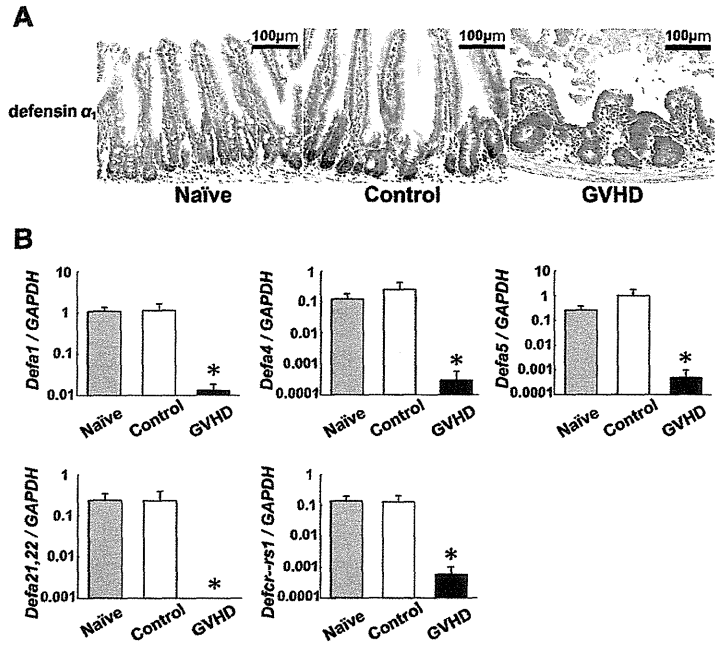

Figure 2. Decreased expression of Paneth cell–derived α-defensins in GVHD. Lethally irradiated B6D2F1 mice were transplanted with 5×10^6 TCD BM without (control group) or with (GVHD group) 2×10^6 T cells from B6 donors. Small intestines were isolated from mice 7 days after BMT. (A) Immunohistochemical staining for defensin α_1 (brown). Magnification: 100×. Bars, 100 μm. (B) RNA was extracted from samples and quantitative real-time PCR analysis for enteric defensins including *Defa1*, *Defa4*, *Defa5*, *Defa21,22*, and *Defcr-rs1* was performed (n = 6 / group). Data are representative of 2 similar experiments and are shown as mean ± SE (*$P < .05$).

were significantly and constantly lower compared with those in controls after BMT (Figure 1F).

α-Defensins are the major antimicrobial peptides produced by Paneth cells.[23] We evaluated the expression levels of enteric defensin families in the small intestines. Defensin α_1 expression was limited in Paneth cells in the crypts of naive mice (Figure 2A). Expression of defensin α_1 was preserved in controls 7 days after BMT but was severely suppressed in mice with GVHD. Quantitative real-time PCR analysis of the terminal ileum confirmed the reduced expression of *defensin-α_1 (Defa1)* and other enteric defensin family members, including *Defa5*, *Defa21,22*, and *defensin α-related sequence 1 (Defa-rs1)* in the small intestine of GVHD mice (Figure 2B). These results demonstrate that GVHD targets Paneth cells and limits the expression of Paneth cell–derived defensin family members.

Perturbation of normal intestinal microbiota in GVHD

Paneth cell–derived α-defensins are essential regulators of the microbiota composition in the intestine.[11] α-defensins have selective bactericidal activity against noncommensals, whereas exhibiting minimal bactericidal activity against commensals.[28,29] We therefore hypothesized that the reduced expression of α-defensins results in dysbiosis in the intestinal microbial community. To test this hypothesis, we evaluated changes in the gut flora during the course of GVHD in a B6 → B6D2F1 murine model of BMT without administering any antibiotic or immunosuppressive drugs. Before and after BMT, fecal pellets were collected from each mouse once per week. The composition of the intestinal microflora was determined by RFLP analysis of bacteria-specific 16S rRNA genes that were constructed from each sample of fecal pellets.[30,31] Representative RFLP analysis is shown in Figure 3A. Each unique RFLP pattern is designated by an OTU that corresponds to specific species of bacteria. The peak height of each OTU indicates its relative quantity among the intestinal microflora and the number of OTUs indicates the diversity of flora. Before BMT, multiple OTUs were observed with little interindividual variation among the RFLP patterns (Figure 3A left panels). Seven days after BMT, numbers of OTUs were slightly decreased with little changes in the RFLP patterns in controls (Figure 3A right top panels); however, in the mice with GVHD, the number of OTUs decreased and the peak heights of OTUs were markedly reduced, with the exception of an aberrantly high peak at 368 bp (Figure 3A right bottom panels). Sequence analysis of subclones from a representative animal from GVHD group showed that proportions of both Firmicutes and Bacteroidetes, which are the major enteric commensals,[12,15] were decreased in mice with GVHD on day 7 compared with those before BMT (Firmicutes; 22.9% vs 52.1%, Bacteroidetes; 2.1% vs 13.5%, respectively).

These compositional changes in the intestinal microflora were consistently observed in all mice with GVHD. Diversity of the microbial community, which corresponds to the RFLP banding patterns, was significantly reduced in mice with GVHD at all time points, as assessed by the Simpson index of diversity,[26] Shannon diversity index,[27] and the number of OTUs counted (Figure 3B-D).

Overwhelming outgrowth of *E coli* in mice with GVHD

A single high peak at 368bp was noted in mice with GVHD (Figure 3A arrows). To identify the bacteria included at this OTU, plasmid DNA from the corresponding clone was purified. DNA sequencing showed a high similarity to 16S rRNA from *E coli* with a similarity rate of more than 99.5%. The proportion of *E coli* in the microbiota, which was defined as the ratio of the area of OTU for *E coli* to the total areas of all OTUs, was dramatically higher 7 days after BMT and remained higher in mice with GVHD throughout the entire observation period; however, *E coli* remained to be a small portion of the microbial population in controls (Figure 3E). Next, we evaluated whether the high levels of *E coli* in the intestine could be associated with the development of systemic infection in mice with GVHD. Seven days after BMT, mLNs and livers were harvested. *E coli* was identified from samples taken from mice with GVHD, but not the controls. The number of CFUs of *E coli* was significantly higher in the mLNs and liver of mice with GVHD than those in controls (Figure 3F-G). Serum LPS levels were also significantly higher in mice with GVHD than in controls (Figure 3H).

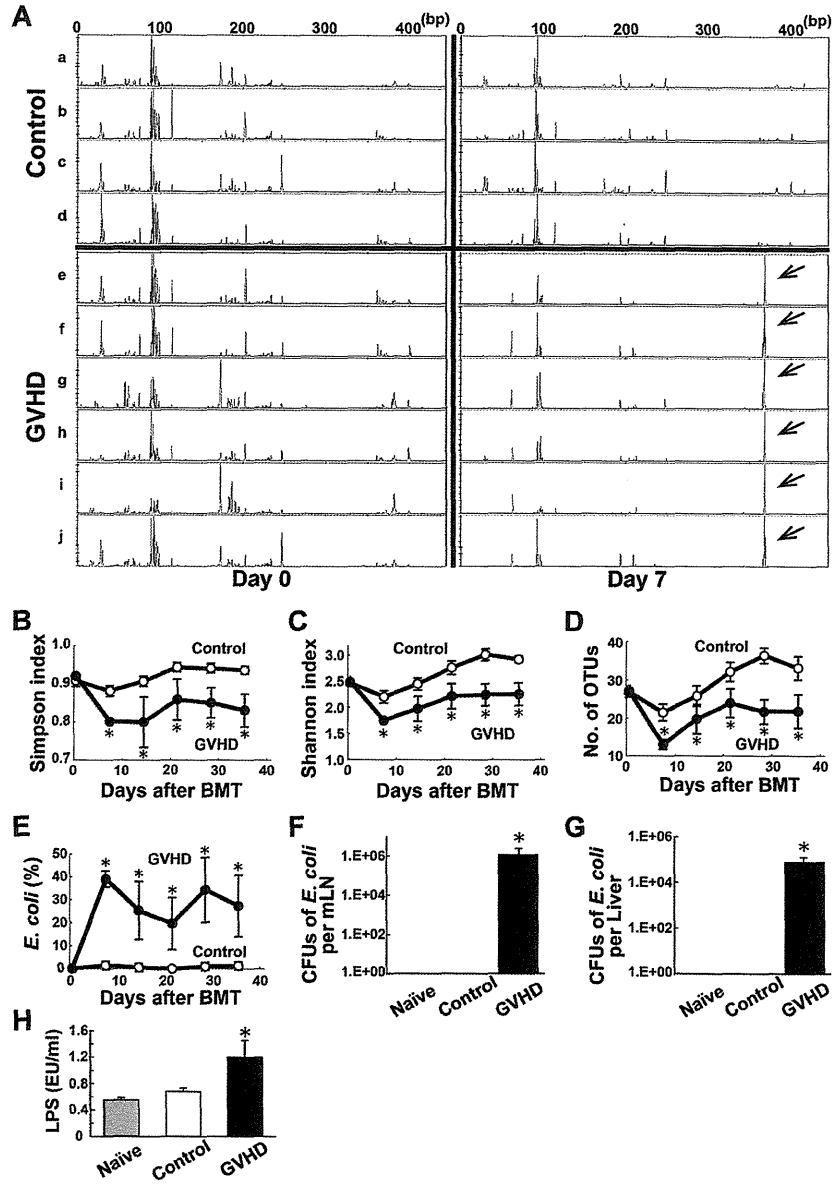

Figure 3. Perturbation of normal intestinal microbiota in GVHD. Fecal pellets were collected before and after a B6 → B6D2F1 BMT weekly and intestinal microbiota was characterized by RFLP analysis of 16S rRNA gene libraries constructed from each sample of fecal pellets and digested with *Hhal* (n = 6 / group). (A) Representative RFLP patterns are shown in control group (a-d) and GVHD group (e-j). Left panels indicate before BMT; right panels, 7 days after BMT. Arrows indicate an OTU for *Escherichia coli*. (B-D) Time course changes in flora diversity after BMT determined by using Simpson index (B), Shannon index (C), and numbers of OTUs (D). (E) Time course changes in the proportion of *E coli*. (F-G) Samples of mLNs and liver were harvested on day 7 and CFUs of *E coli* were enumerated by the culture-based and microbiologic identification method. (H) Serum LPS levels on day 7. Data are representative of 3 similar experiments and are shown as mean ± SE (*$P < .05$).

The composition of intestinal microflora in animals can differ depending on the environment and other factors.[32] Therefore, we used mice purchased from multiple vendors; however, the resulting patterns of dysbiosis were similar, regardless of the origin source of the mice. In addition, we found similar changes in the intestinal microbiota of another haplotype, the mismatched B6 → B6C3F1 (H-$2^{b/k}$) model of BMT. Diversity of intestinal flora was lost with an outgrowth of *E coli* 7 days after BMT and thereafter only in mice with GVHD (data not shown).

Association between changes in intestinal microbiota and GVHD severity

Further studies were conducted to determine whether there could be an association between the magnitude of changes observed in the intestinal flora and GVHD severity. Diversity of the flora, as determined by the Simpson index, Shannon index, and the number of OTUs was inversely correlated with GVHD severity (Figure 4A-C). On the other hand, the proportion of *E coli* in the intestinal flora was positively correlated with GVHD severity (Figure 4D).

Delayed alteration in intestinal microbial diversity after MHC-matched BMT

To further confirm that our observations were not strain or model dependent, we evaluated whether the observed changes in the intestinal flora could be observed in a clinically relevant, MHC-matched, and minor histocompatibility antigen-mismatched C3H.Sw (H-2^b) → B6 (H-2^b) model of BMT, in which GVHD developed more slowly and was less severe compared with the MHC-mismatched models of GVHD (Figure 5A-B).[33] Again, normal microbial diversity was lost in mice with GVHD and *E coli* levels were higher at 2 weeks after BMT and thereafter (Figure 5C-F). Thus, changes in the intestinal microbiota occurred more slowly in this model, at least compared with the MHC-mismatched model of GVHD; furthermore, the changes occurred in parallel with the

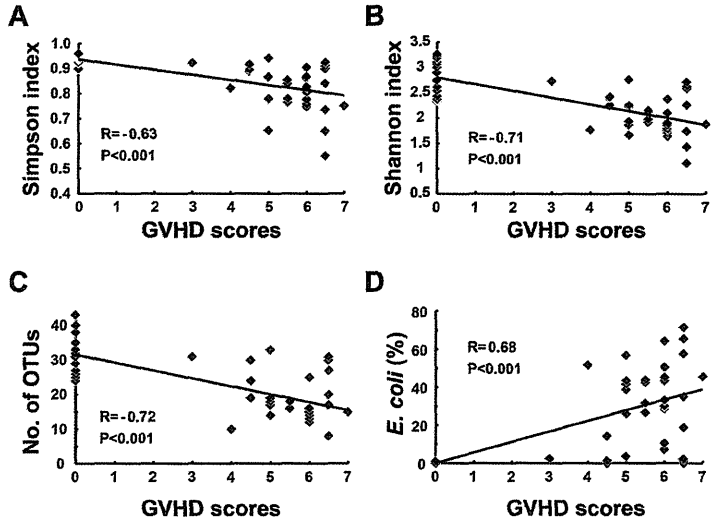

Figure 4. Correlation between the degree of flora changes and GVHD severity. Lethally irradiated B6D2F1 mice were transplanted with TCD BM with T cells from B6 donors (n = 6 / group). Fecal pellets were collected at day 0 and weekly thereafter and intestinal microbiota was characterized by RFLP analysis. Clinical GVHD scores and various parameters of the flora diversity and the proportion of *E coli* in the intestinal flora at various time points from each mice were plotted. Correlations of GVHD clinical scores and Simpson index (A), Shannon index (B), numbers of OTUs (C), and proportion of *E coli* (D). The regression line was plotted with all data. Data from 2 independent experiments were combined. R: correlation coefficient.

slower development of GVHD. It should be noted that normal flora diversity was recovered and *E coli* returned to a normally small population among the intestinal microbiota late after BMT, as GVHD severity reduced. No mortality was observed in allogeneic animals after regaining normal intestinal flora.

Loss of Paneth cells and the dysbiosis by a mechanism independent on conditioning

We addressed whether GVHD mediates Paneth cell injury and the alteration of the composition of the intestinal flora by a mechanism dependent on radiation-induced intestinal tract damage in the B6 → B6D2F1 BMT model without conditioning, as previously described.[7] Unirradiated B6D2F1 mice were intravenously injected with 12×10^7 splenocytes from syngeneic or allogeneic B6 donors on day 0. In this model, GVHD occurred early after BMT at a peak around day 20 but was spontaneously improved (Figure 6A-C). Numbers of Paneth cells were markedly reduced 2 weeks after BMT but gradually returned to normal levels thereafter in allogeneic animals (Figure 6D). The changes in the intestinal microbiota occurred in parallel with the degree of GVHD severity and Paneth cell injury; normal microbial diversity was lost with the outgrowth of *E coli*, but was gradually restored later after BMT in allogeneic animals (Figure 6E-H).

Oral administration of antibiotics inhibited the outgrowth of *E coli* and ameliorated GVHD

Finally, we evaluated whether modifying the enteric flora using oral antibiotics could ameliorate GVHD. Lethally irradiated B6D2F1 mice were transplanted with 5×10^6 TCD BM cells with or without 2×10^6 T cells from B6-Ly5.1 (CD45.1$^+$) donors. Polymyxin B (PMB), an antibiotic primarily effective against gram-negative bacteria, was administered by daily oral gavage at a dose of 100 mg/kg from day −4 until day 28 after BMT. Analysis of fecal pellets 7 days after BMT showed that the outgrowth of *E coli* was inhibited in mice treated with PMB compared with those treated with diluent (Figure 7A). PMB suppressed the outgrowth of *E coli* during PMB treatment; however, *E coli* levels increased after cessation of PMB treatment (Figure 7B). Notably, administration of PMB significantly reduced mortality and morbidity of GVHD (Figure 7C-D). Donor (CD45.1$^+$) T-cell expansion (Figure 7E) and pathology scores of the small intestine (Figure 7F) were significantly reduced in PMB-treated mice compared with those in controls.

Discussion

Intestinal GVHD is critical for determining the outcome of allogeneic BMT. Paneth cells are essential regulators of the

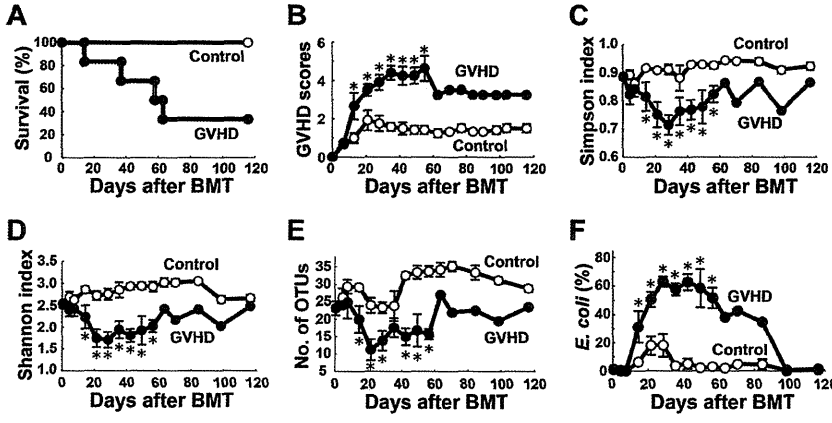

Figure 5. Delayed impairment of the intestinal ecology after MHC-matched BMT. B6 mice were transplanted with 5×10^6 TCD BM without (control group) or with (GVHD group) 2×10^6 T cells from C3H.Sw donors after 12 Gy TBI (n = 6/group). (A-B) Survival (A) and clinical GVHD scores (B, mean ± SE) in control group and GVHD group. Data are representative of 3 similar experiments. (C-F) Fecal pellets were collected once per week after BMT and intestinal microflora was characterized by RFLP analysis of 16S rRNA genes constructed from each sample of fecal pellets and digested with *Hha*I. Time course changes in flora diversity determined by Simpson index (C), Shannon index (D), and numbers of OTUs (E). (F) Time course changes in the proportion of *E coli*. Data are representative of 3 similar experiments and are shown as mean ± SE (*$P < .05$).

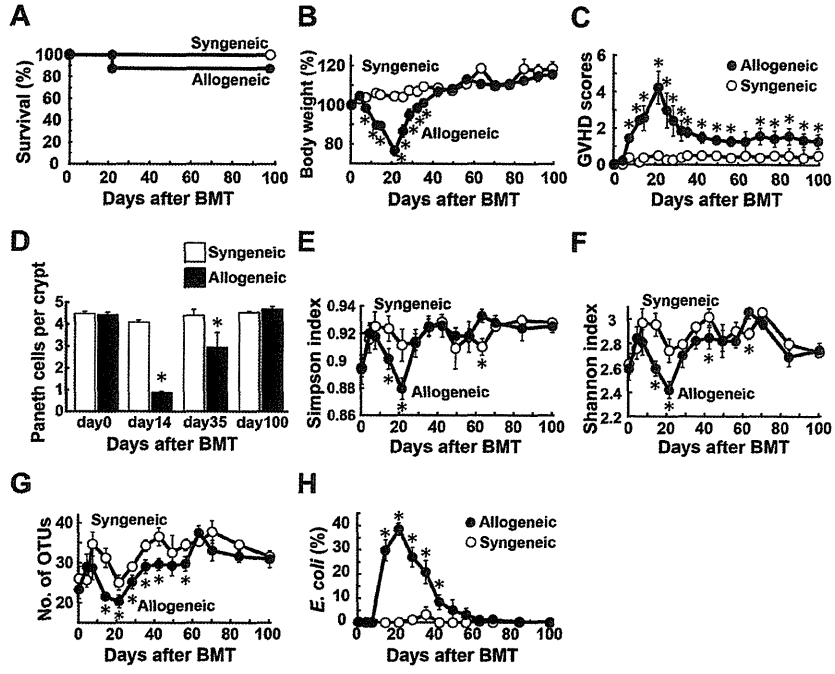

Figure 6. Paneth cell injury and the dysbiosis developed by a mechanism independent on conditioning. Unirradiated B6D2F1 mice were transplanted with 12×10^7 splenocytes from syngeneic or allogeneic MHC-mismatched B6 donors on day 0 (n = 6/group). Survival (A), changes in body weight (B, mean ± SE), clinical GVHD scores (C, mean ± SE), and (D) quantification of Paneth cells per crypt in the small intestine were shown. (E-H) Fecal pellets were collected before and after BMT weekly and intestinal microbiota was characterized by RFLP analysis of 16S rRNA gene libraries constructed from each sample of fecal pellets and digested with *Hhal*. Time course changes in flora diversity determined by using Simpson index (E), Shannon index (F), numbers of OTUs (G), and the proportion of *E coli* (H). Data from 2 independent experiments were combined and are shown as mean ± SE.

composition of commensal microbiota in the intestine, and they maintain the intestinal microbial environment by secreting various microbial peptides. In this study, we found that damage to Paneth cells by GVHD results in dramatically reduced expression of α-defensins in the small intestines and perturbed normal intestinal environment. These changes occurred in the absence of conditioning irradiation, thus indicating a mechanism dependent on allogeneic T-cell responses. However, Paneth cell loss occurred earlier and more prolonged in mice receiving irradiation than in unirradiated mice, suggesting that conditioning enhanced Paneth cell damage directly and indirectly by accelerating GVHD. The diversity of the intestinal microflora was lost with overwhelming expansion of specific bacteria, such as *E coli*, which are normally a very small proportion of the intestinal microbial communities. Paneth cells secret α-defensins into the intestinal lumen within minutes after sensing gram-negative and gram-positive bacteria and their components, such as LPS, through activation of pattern recognition receptors.[23,34] α-defensins are the most potent antimicrobial peptides and account for 70% of the bactericidal peptide activity released from Paneth cells.[11,23] α-Defensins are released in the small bowel lumen and persist as intact and functional forms throughout the intestinal tract.[35] Thus, they shape the composition of the microbiota in the entire intestine. Importantly, α-defensins have selective bactericidal activity against noncommensals, such as *Salmonella enterica*, *E coli*, *Klebsiella pneumoniae*, and *Staphylococcus aureus*, although exhibiting minimal bactericidal activity against commensals.[28,29] Such bacteria-dependent bactericidal activities of α-defensins are in tune with intestinal environment and may explain why the absence of α-defensins causes the alterations in the intestinal microbiota in GVHD. Because commensals have a profound influence on nutritional, physiologic, and metabolic function of the host,[14,36,37] reduction of commensals may have ill effects on the host with GVHD. In this study, *E coli* was the dominant enteric microbe in mice with GVHD among multiple strains of mice. However, the dominant species may differ between studies because of the differences in several factors, including differences in the maintenance protocols used to feed and care for the experimental animals.[32] Nonetheless, our study confirms and further extends a recent study showing the intestinal flora change, with an increase in gram-negative *Enterobacteriaceae* family members including *E coli*, after allogeneic BMT in mice.[18]

Alteration of the intestinal microbiota has been shown in experimental and clinical inflammatory bowel diseases, allergies, diabetes, and obesity.[13,38-42] This study provides several lines of evidence that suggest a close association between dysbiosis and GVHD. Mice without GVHD maintained normal microbiota after BMT, and dysbiosis only occurred in mice with GVHD, independent of the murine models used. The normal intestinal environment was never restored as long as severe GVHD persisted, but was restored when tolerance was induced after transplant. In mice with GVHD, the degree of changes to the microflora was significantly correlated to GVHD severity and MHC disparity between the donor and recipient. Furthermore, modifying enteric flora by oral administration of antibiotics inhibited the outgrowth if *E coli* and ameliorated GVHD. The flora shift toward the widespread prevalence of gram-negative bacteria increases the translocation of LPS, the major component of the outer membrane of gram-negative bacteria, into systemic circulation and further accelerates GVHD by stimulates production of inflammatory cytokines, such as TNF-α and IL-1, which are critical effector molecules that mediate GVHD.[22,43-45] Thus, GVHD and the dysbiosis can lead to a positive feedback loop that increases the translocation of LPS, thereby resulting in further cytokine production, progressive intestinal injury, and systemic GVHD acceleration. Earlier seminal studies in the 1960s-1970s suggested that GVHD is reduced in germfree mice or by treatment with poorly absorbable antibiotics.[3-6] A recent study also demonstrated that modifying the enteric flora using a probiotic microorganism reduced GVHD in mice.[46] Thus, our study again highlights an important role of oral antibiotics administration on GVHD. Our study demonstrated that dominant bacteria in the intestinal microbiota cause systemic infection. There was a microbiologic evidence of infection in mice with severe GVHD and a correlation between severity of infection and GVHD, thus suggesting that severe bacteremia, probably caused by the translocation of enteric bacteria, can also contribute to GVHD mortality, as previously suggested.[6,46] Indeed, septicemia by gram-negative rods

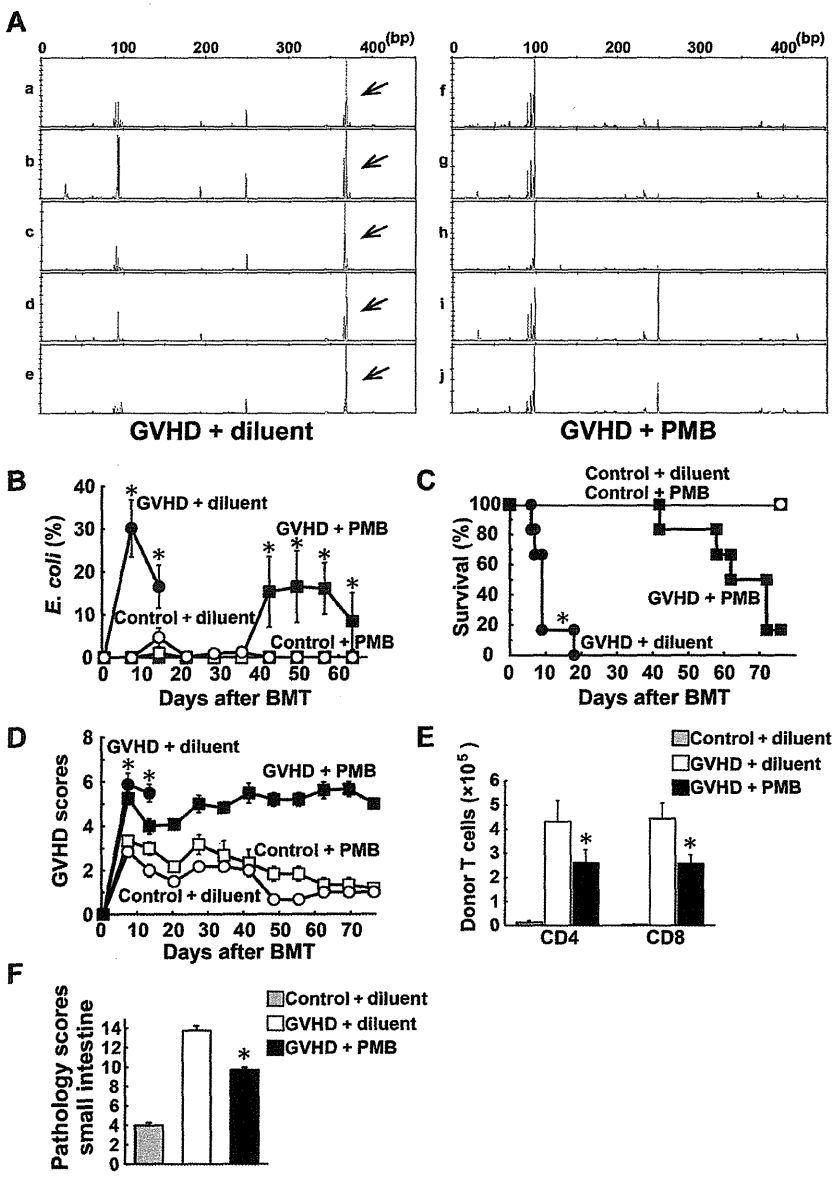

Figure 7. Oral administration of polymyxin B ameliorated GVHD. Lethally irradiated B6D2F1 mice were transplanted with 5×10^6 TCD BM without or with 2×10^6 T cells from B6 or B6-Ly5.1 (CD45.1$^+$) donors. Polymyxin B (PMB; 100 mg/kg) or diluent was administered by daily oral gavage from day −4 until day 28 after BMT. (A) Fecal pellets were collected once per week after BMT and intestinal microflora was characterized by RFLP analysis of 16S rRNA genes constructed from each sample of fecal pellets and digested with *HhaI*. Representative RFLP patterns are shown in mice with GVHD receiving diluent (a-e) and those with PMB (f-j) 7 days after BMT. Arrows indicate an OTU for *E coli*. (B) Time course changes in the proportion of *E coli* (n = 6-12 / group). Survival (C) and clinical GVHD scores (D, mean ± SE) after BMT are shown (n = 6-12/group). Data from 2 independent experiments were combined. (E) Numbers of donor (CD45.1$^+$) T cells in mLNs on day 5 (n = 20/group). (F) Pathology scores of the small intestine on day 7 (n = 20/group). Data from 3 independent experiments were combined and are shown as mean ± SE (*$P < .05$).

is one of the most frequent causes of death in patients with severe intestinal GVHD.

There are other interfaces that exist between the environment and the host, such as the skin and airways. Epithelial cells in these tissues can also release antimicrobial peptides such as β-defensins in response to bacteria and LPS.[47] GVHD-mediated epithelial cell damage of these tissues may also impair the local secretion of antimicrobial peptides, leading to aberrant overgrowth of pathogens and development of dermal infections or pneumonia, which are frequently observed in patients with GVHD. Furthermore, the development of these pathologic conditions may be associated with the unique tissue specificity of GVHD for tissues that are in contact with high microbial loads, such as the skin, liver, intestine, and lung.

Intestinal epithelial cells are continuously regenerated from ISCs, which are required to regenerate damaged sections of the intestinal epithelium.[48] Paneth cells are derived from ISCs and serve as a niche for ISCs.[8] Our previous[7] and current studies addressed intestinal GVHD at the cellular level, and demonstrated that ISCs and their niche Paneth cells could survive pretransplant conditioning and regenerate injured epithelium by conditioning in the absence of GVHD. However, both ISCs and Paneth cells are targeted by GVHD, resulting in an impairment of the physiologic repair mechanisms of injured epithelium, although it remains to be elucidated whether Paneth cell loss is induced by direct cytotoxicity to Paneth cell itself or secondary to the loss of ISCs. This phenomenon may explain the prolonged and refractory nature of clinical intestinal GVHD. These new insights will help to establish new therapeutic strategies that can be used to prevent and treat GVHD and related infections and improve the clinical outcome of allogeneic BMT.

Acknowledgments

This study was supported by grants from Japan Society for the Promotion of Science (JSJP) KAKENHI (23659490 to T.T., 23390193 to T.A., and 22592029 to K.N.), Health and Labor Science Research Grants (T.T.), the Foundation for Promotion of Cancer Research (Tokyo, Japan; to T.T.), the Knowledge Cluster, Sapporo Bio-S from Ministry of

Education, Culture, Sports, Science and Technology (MEXT; Tokyo, Japan; to T.A.), Yakult Bio-Science Foundation (Tokyo, Japan; to Y.E.), and SENSHIN Medical Research Foundation (to T.T.).

Authorship

Contribution: Y.E. and T.T. developed the conceptual framework of the study, designed the experiments, conducted studies, analyzed data, and wrote the paper; S.T., H.O., S. Shimoji, K.N., H.U., S. Shimoda, and H.I. conducted experiments; and N.S., T.A., and K.A. supervised experiments.

Conflict-of-interest disclosure: The authors declare no competing financial interests.

Correspondence: Takanori Teshima, Center for Cellular and Molecular Medicine, Kyushu University Hospital, 3-1-1 Maidashi, Higashi-ku, Fukuoka 812-8582, Japan; e-mail: tteshima@cancer.med.kyushu-u.ac.jp.

References

1. Bossaer JB, Hall PD, Garrett-Mayer E. Incidence of vancomycin-resistant enterococci (VRE) infection in high-risk febrile neutropenic patients colonized with VRE. *Support Care Cancer.* 2010; 19(2):231-237.
2. Winston DJ, Gale RP, Meyer DV, Young LS. Infectious complications of human bone marrow transplantation. *Medicine.* 1979;58(1):1-31.
3. van Bekkum D, Vos O. Treatment of secondary disease in radiation chimaeras. *Int J Radiat Biol.* 1961;3:173-181.
4. Jones JM, Wilson R, Bealmear PM. Mortality and gross pathology of secondary disease in germ-free mouse radiation chimeras. *Radiation Res.* 1971;45(3):577-588.
5. van Bekkum DW, Roodenburg J, Heidt PJ, van der Waaij D. Mitigation of secondary disease of allogeneic mouse radiation chimeras by modification of the intestinal microflora. *J Nat Cancer Inst.* 1974;52(2):401-404.
6. Heit H, Heit W, Kohne E, Fliedner TM, Hughes P. Allogeneic bone marrow transplantation in conventional mice: I. Effect of antibiotic therapy on long term survival of allogeneic chimeras. *Blut.* 1977;35(2):143-153.
7. Takashima S, Kadowaki M, Aoyama K, et al. The Wnt agonist R-spondin1 regulates systemic graft-versus-host disease by protecting intestinal stem cells. *J Exp Med.* 2011;208(2):285-294.
8. Sato T, van Es JH, Snippert HJ, et al. Paneth cells constitute the niche for Lgr5 stem cells in intestinal crypts. *Nature.* 2011;469(7330):415-418.
9. Selsted ME, Harwig SS. Determination of the disulfide array in the human defensin HNP-2. A covalently cyclized peptide. *J Biol Chem.* 1989; 264(7):4003-4007.
10. Ganz T, Selsted ME, Lehrer RI. Defensins. *Eur J Haematol.* 1990;44(1):1-8.
11. Salzman NH, Hung K, Haribhai D, et al. Enteric defensins are essential regulators of intestinal microbial ecology. *Nat Immunol.* 2010;11(1):76-83.
12. Eckburg PB, Bik EM, Bernstein CN, et al. Diversity of the human intestinal microbial flora. *Science.* 2005;308(5728):1635-1638.
13. Qin J, Li R, Raes J, et al. A human gut microbial gene catalogue established by metagenomic sequencing. *Nature.* 2010;464(7285):59-65.
14. Hill DA, Artis D. Intestinal bacteria and the regulation of immune cell homeostasis. *Ann Rev Immunol.* 2010;28:623-667.
15. Zoetendal EG, Akkermans AD, De Vos WM. Temperature gradient gel electrophoresis analysis of 16S rRNA from human fecal samples reveals stable and host-specific communities of active bacteria. *Appl Environ Microbiol.* 1998;64(10): 3854-3859.
16. Kurokawa K, Itoh T, Kuwahara T, et al. Comparative metagenomics revealed commonly enriched gene sets in human gut microbiomes. *DNA Res.* 2007;14(4):169-181.
17. Hooper LV, Macpherson AJ. Immune adaptations that maintain homeostasis with the intestinal microbiota. *Nature Rev Immunol.* 2010;10(3):159-169.
18. Heimesaat MM, Nogai A, Bereswill S, et al. MyD88/TLR9 mediated immunopathology and gut microbiota dynamics in a novel murine model of intestinal graft-versus-host disease. *Gut.* 2010; 59(8):1079-1087.
19. Ubeda C, Taur Y, Jenq RR, et al. Vancomycin-resistant Enterococcus domination of intestinal microbiota is enabled by antibiotic treatment in mice and precedes bloodstream invasion in humans. *J Clin Invest.* 2010;120(12):4332-4341.
20. Cooke KR, Kobzik L, Martin TR, et al. An experimental model of idiopathic pneumonia syndrome after bone marrow transplantation. I. The roles of minor H antigens and endotoxin. *Blood.* 1996;88: 3230-3239.
21. Asakura S, Hashimoto D, Takashima S, et al. Alloantigen expression on non-hematopoietic cells reduces graft-versus-leukemia effects in mice. *J Clin Invest.* 2010;120(7):2370-2378.
22. Teshima T, Ordemann R, Reddy P, et al. Acute graft-versus-host disease does not require alloantigen expression on host epithelium. *Nat Med.* 2002;8(6):575-581.
23. Ayabe T, Satchell DP, Wilson CL, Parks WC, Selsted ME, Ouellette AJ. Secretion of microbicidal alpha-defensins by intestinal Paneth cells in response to bacteria. *Nat Immunol.* 2000;1(2): 113-118.
24. Li F, Hullar MA, Lampe JW. Optimization of terminal restriction fragment polymorphism (TRFLP) analysis of human gut microbiota. *J Microbiol Methods.* 2007;68(2):303-311.
25. Hayashi H, Takahashi R, Nishi T, Sakamoto M, Benno Y. Molecular analysis of jejunal, ileal, caecal and recto-sigmoidal human colonic microbiota using 16S rRNA gene libraries and terminal restriction fragment length polymorphism. *J Med Microbiol.* 2005;54(Pt 11):1093-1101.
26. Simpson EH. Measurement of diversity. *Nature.* 1949;163:688.
27. Shannon C. A mathematical theory of communication. *Bell System Technol J.* 1948;27:379-423.
28. Ouellette AJ, Hsieh MM, Nosek MT, et al. Mouse Paneth cell defensins: primary structures and antibacterial activities of numerous cryptdin isoforms. *Infect Immun.* 1994;62(11):5040-5047.
29. Masuda K, Sakai N, Nakamura K, Yoshioka S, Ayabe T. Bactericidal activity of mouse alpha-defensin cryptdin-4 predominantly affects noncommensal bacteria. *J Innate Immun.* 2011;3(3): 315-326.
30. Liu WT, Marsh TL, Cheng H, Forney LJ. Characterization of microbial diversity by determining terminal restriction fragment length polymorphisms of genes encoding 16S rRNA. *Appl Environ Microbiol.* 1997;63(11):4516-4522.
31. Hayashi H, Sakamoto M, Benno Y. Phylogenetic analysis of the human gut microbiota using 16S rDNA clone libraries and strictly anaerobic culture-based methods. *Microbiol Immunol.* 2002; 46(8):535-548.
32. Ivanov II, Atarashi K, Manel N, et al. Induction of intestinal Th17 cells by segmented filamentous bacteria. *Cell.* 2009;139(3):485-498.
33. Shlomchik WD, Couzens MS, Tang CB, et al. Prevention of graft versus host disease by inactivation of host antigen-presenting cells. *Science.* 1999;285(5426):412-415.
34. Vaishnava S, Behrendt CL, Ismail AS, Eckmann L, Hooper LV. Paneth cells directly sense gut commensals and maintain homeostasis at the intestinal host-microbial interface. *Proc Natl Acad Sci U S A.* 2008; 105(52):20858-20863.
35. Mastroianni JR, Ouellette AJ. Alpha-defensins in enteric innate immunity: functional Paneth cell alpha-defensins in mouse colonic lumen. *J Biol Chem.* 2009;284(41):27848-27856.
36. Hooper LV, Midtvedt T, Gordon JI. How host-microbial interactions shape the nutrient environment of the mammalian intestine. *Annu Rev Nutr.* 2002;22:283-307.
37. Bäckhed F, Ley RE, Sonnenburg JL, Peterson DA, Gordon JI. Host-bacterial mutualism in the human intestine. *Science.* 2005;307(5717):1915-1920.
38. Ley RE, Turnbaugh PJ, Klein S, Gordon JI. Microbial ecology: human gut microbes associated with obesity. *Nature.* 2006;444(7122):1022-1023.
39. Turnbaugh PJ, Ley RE, Mahowald MA, Magrini V, Mardis ER, Gordon JI. An obesity-associated gut microbiome with increased capacity for energy harvest. *Nature.* 2006;444(7122):1027-1031.
40. Manichanh C, Rigottier-Gois L, Bonnaud E, et al. Reduced diversity of faecal microbiota in Crohn's disease revealed by a metagenomic approach. *Gut.* 2006;55(2):205-211.
41. Bollyky PL, Bice JB, Sweet IR, et al. The toll-like receptor signaling molecule Myd88 contributes to pancreatic beta-cell homeostasis in response to injury. *PLoS One.* 2009;4(4):e5063.
42. Penders J, Thijs C, van den Brandt PA, et al. Gut microbiota composition and development of atopic manifestations in infancy: the KOALA Birth Cohort Study. *Gut.* 2007;56(5):661-667.
43. Hill GR, Ferrara JL. The primacy of the gastrointestinal tract as a target organ of acute graft-versus-host disease: rationale for the use of cytokine shields in allogeneic bone marrow transplantation. *Blood.* 2000;95(9):2754-2759.
44. Nestel FP, Price KS, Seemayer TA, Lapp WS. Macrophage priming and lipopolysaccharide-triggered release of tumor necrosis factor alpha during graft-versus-host disease. *J Exp Med.* 1992;175:405-413.
45. Cooke KR, Gerbitz A, Crawford JM, et al. LPS antagonism reduces graft-versus-host disease and preserves graft-versus-leukemia activity after experimental bone marrow transplantation. *J Clin Invest.* 2001;107(12):1581-1589.
46. Gerbitz A, Schultz M, Wilke A, et al. Probiotic effects on experimental graft-versus-host disease: let them eat yogurt. *Blood.* 2004;103(11):4365-4367.
47. Bals R, Wang X, Meegalla RL, et al. Mouse beta-defensin 3 is an inducible antimicrobial peptide expressed in the epithelia of multiple organs. *Infect Immun.* 1999;67(7):3542-3547.
48. Sato T, Vries RG, Snippert HJ, et al. Single Lgr5 stem cells build crypt-villus structures in vitro without a mesenchymal niche. *Nature.* 2009; 459(7244):262-265.

Regular Article

LYMPHOID NEOPLASIA

PU.1 is a potent tumor suppressor in classical Hodgkin lymphoma cells

Hiromichi Yuki,[1] Shikiko Ueno,[1] Hiro Tatetsu,[1] Hiroaki Niiro,[2] Tadafumi Iino,[2] Shinya Endo,[1] Yawara Kawano,[1] Yoshihiro Komohara,[3] Motohiro Takeya,[3] Hiroyuki Hata,[1] Seiji Okada,[4] Toshiki Watanabe,[5] Koichi Akashi,[2] Hiroaki Mitsuya,[1] and Yutaka Okuno[1]

[1]Department of Hematology, Kumamoto University of Medicine, Kumamoto, Japan; [2]Medicine and Biosystemic Science, Kyushu University Graduate School of Medical Sciences, Fukuoka, Japan; [3]Department of Cell Pathology, Kumamoto University of Medicine, Kumamoto, Japan; [4]Division of Hematopoiesis, Center for AIDS Research, Kumamoto University, Kumamoto, Japan; and [5]Graduate School of Frontier Sciences, University of Tokyo, Tokyo, Japan

Key Points

- PU.1 is a potent tumor suppressor in cHL cells and the induction of PU.1 is a possible therapeutic option for patients with cHL.

PU.1 has previously been shown to be down-regulated in classical Hodgkin lymphoma (cHL) cells via promoter methylation. We performed bisulfite sequencing and proved that the promoter region and the −17 kb upstream regulatory element of the *PU.1* gene were highly methylated. To evaluate whether down-regulation of PU.1 is essential for the growth of cHL cells, we conditionally expressed PU.1 in 2 cHL cell lines, L428 and KM-H2. Overexpression of PU.1 induced complete growth arrest and apoptosis in both cell lines. Furthermore, in a Hodgkin lymphoma tumor xenograft model using L428 and KM-H2 cell lines, overexpression of PU.1 led to tumor regression or stable disease. Lentiviral transduction of PU.1 into primary cHL cells also induced apoptosis. DNA microarray analysis revealed that among genes related to cell cycle and apoptosis, *p21 (CDKN1A)* was highly up-regulated in L428 cells after PU.1 induction. Stable knockdown of p21 rescued PU.1-induced growth arrest in L428 cells, suggesting that the growth arrest and apoptosis observed are at least partially dependent on p21 up-regulation. These data strongly suggest that PU.1 is a potent tumor suppressor in cHL and that induction of PU.1 with demethylation agents and/or histone deacetylase inhibitors is worth exploring as a possible therapeutic option for patients with cHL. (*Blood.* 2013;121(6):962-970)

Introduction

Hodgkin lymphoma is a B-cell malignancy that occurs frequently in the white population, and is relatively rare within Japanese and other Asian populations.[1] To date, the combination of chemotherapy and irradiation has led to a dramatic improvement in both progression-free survival and overall survival of stage I and II patients, which now exceeds 90%.[2] In contrast, the prognosis of the remaining patients who relapse or fail to make complete remission, and in stage III and IV patients, is relatively poor.[3-9] In addition, patients who achieve long-term disease-free survival frequently have infertility and secondary malignancies, including breast cancer and cardiac failure, which are related to chemotherapeutic agents and radiation therapies.[10-12] Therefore, the development of new therapeutic strategies is necessary to improve clinical outcome and reduce the long-term side effects of current treatments in these patients. Nevertheless, our understanding of the mechanisms underlying the pathogenesis of Hodgkin lymphoma, which are necessary for the generation of novel, molecularly targeted agents, remains incomplete. It is known that both alleles of *tumor necrosis factor, α-induced protein 3 (TNFAIP3)(A20)* are deleted in a third of patients with Hodgkin lymphoma of nodular sclerosis histology and in the classic Hodgkin lymphoma (cHL) cell line, KM-H2.[13]

Hodgkin lymphoma is subdivided into cHL, which constitutes the majority of patients (95%), and nodular lymphocyte predominant Hodgkin lymphoma.[1] In cHL, lymphoma cells do not express the B cell–specific surface antigens, CD19 and CD20, or the B cell–specific transcription factors, Bob.1, PU.1, and SpiB.[14,15]

PU.1 is an Ets family transcription factor that is essential for the differentiation of both myeloid and lymphoid cells.[16,17] PU.1 is expressed in granulocytes, monocytes/macrophages, and B cells, but not in erythrocytes or T cells. The expression of *PU.1* requires an upstream regulatory element (URE) located −14 kb and −17 kb upstream of the transcriptional start site of the murine and human *PU.1* genes, respectively, in addition to promoter regulatory elements.[18-20] In murine models, deletion of the −14 kb URE led to down-regulation of PU.1 expression to 20% of wild-type mice, and surprisingly, knockout mice developed acute myeloid leukemia and a B-cell chronic lymphocytic leukemia-like disease.[21,22] These data suggest that PU.1 has tumor suppressor activity in myeloid cells and B cells. We recently reported that PU.1 is down-regulated in a subset of multiple myeloma cells and in most myeloma cell lines. Conditional expression of PU.1 induced complete growth arrest and apoptosis in myeloma cell lines, suggesting that PU.1 is a potent tumor suppressor in multiple myeloma.[20]

Submitted May 21, 2012; accepted October 30, 2012. Prepublished online as *Blood* First Edition paper, December 4, 2012; DOI 10.1182/blood-2012-05-431429.

The online version of this article contains a data supplement.

The publication costs of this article were defrayed in part by page charge payment. Therefore, and solely to indicate this fact, this article is hereby marked "advertisement" in accordance with 18 USC section 1734.

Previous studies have reported that PU.1 is also down-regulated in cHL cells via methylation of the *PU.1* promoter.[23] Therefore, in this study, we evaluated whether PU.1 is tumor suppressor in cHL cells.

Methods

Bisulfite sequencing

Genomic DNA was treated with sodium bisulfite as previously described[20] and subjected to 35 cycles of PCR. A 149-bp *PU.1* promoter-exon1 region, including a PU.1 binding site, was amplified with the primers 5′-GTAGTTTAGGGGGTAGGTTTGAGTT-3′and 5′-AAAAAAAACCC-TTCCATTTTACAC-3′. PCR products were directly sequenced. A 244-bp product encompassing the −17 kb URE, including PU.1 and runt-related transcription factor 1 (RUNX1/AML1) binding sites, which are required for PU.1 expression, was amplified with the primers 5′-ATTTTTTT-GAGGTTTGGTTTAGGTT-3′ and 5′-CTACAACTACCCCTATTTCC-ACATC-3′. Both regions were previously shown to contain CpG islands.[20]

Cell culture

Human Hodgkin lymphoma cell lines L428, KM-H2, L540, HDLM2, and HD-70 and their derivatives were grown in RPMI 1640 medium containing 10% (volume/volume) FBS at 37°C.

Constructs

pCAG20-1, pUHD-3 puromycin and pUHD-10-3 IRES-GFP plasmids were kind gifts from Dr Takumi Era (Division of Molecular Neurobiology, Institute of Molecular Embryology and Genetics, Kumamoto University, Japan).[24] The human PU.1 cDNA was subcloned into the blunt-ended *EcoR*I site of pUHD10-3 IRES-GFP, resulting in pUHD10-3 PU.1-IRES-GFP.

Generation of stable transformants conditionally expressing PU.1

To obtain PU.1-inducible cHL cell lines using the tetracycline-off system, 1×10^7 L428 or KM-H2 cells were cotransfected with 10 μg each of *Sca*I-digested pCAG20-1 and pUHD-3 puromycin plasmids by electroporation. Cells were selected with 1 μg/mL puromycin, and subsequently transfected with 10 μg of *Sca*I-digested pUHD10-3 PU.1-IRES-GFP and 2 μg of *Hin*dIII-digested pPGKneo.[20] After isolation of G418-resistant clones, GFP expression was evaluated after tetracycline removal. On confirmation of GFP expression, these cells were designated L428$^{tetPU.1}$ and KM-H2$^{tetPU.1}$.

Xenograft model

A total of 7×10^6 L428$^{tetPU.1}$ or KM-H2$^{tetPU.1}$ cells were injected subcutaneously into *Rag2*$^{-/-}$*Jak3*$^{-/-}$ *balb/c* mice (n = 16 per group). Mice were given drinking water containing tetracycline (500 μg/mL) 3 days before injection. Subcutaneous tumors were grown to 1- to 2-cm in diameter (~ 30-35 days after injection), and half of the cohort (n = 8) were maintained on tetracycline-treated water, whereas the remaining mice discontinued tetracycline and were given pure water. Tumor size was measured every 7 days.

Primary cHL cells

Primary cells were obtained from lymph node biopsy samples of 3 patients with cHL. Informed consent for sample collection was obtained according to protocols approved by the institutional review boards and in accordance with the Declaration of Helsinki. Primary cHL cells were purified by negative selection using an anti-CD3, CD14, CD16, CD19, CD20, and CD56 antibody cocktail (BioLegend) and antimouse IgG antibody-conjugated magnetic beads (Miltenyi Biotec). After negative selection, the purity of Hodgkin cells was confirmed by May-Giemsa staining and immunostaining with anti-CD30 antibody of cytospin samples or flow cytometry after staining with anti-CD30 antibody.

Lentiviral transduction

The CSII-EF-MCS-IRES-Venus lentiviral vector and packaging constructs, VSV-G Rev and CAG-HIVgp, were purchased from the RIKEN Bio Resource Center. The human PU.1 cDNA was subcloned into *Not*I site of CSII-EF-MCS-IRES-Venus. Virus was produced and cells were infected as previously described (http://www.brc.riken.jp/lab/cfm/Subteam_for_Manipulation_of_Cell_Fate/Home.html).[25,26]

DNA microarray analysis

Total RNA was extracted from L428$^{tetPU.1}$ and KM-H2$^{tetPU.1}$ cells using Trizol reagent at 3 different time points: days 0, 1, and 3 after tetracycline removal. RNA was hybridized to Illumina:Sentrix Human-6 Expression BeadChips or Illumina HumanHT-12 Version 4 Expression BeadChips, according to the manufacturer's instructions. Gene expression profiles were analyzed using GeneSpring Version 12.0 software.[27] Data for L428$^{tetPU.1}$ cells are available at the Gene Expression Omnibus under accession number GSE42437; data for KM-H2$^{tetPU.1}$ cells are available under GSE42440.

Real-time PCR

Quantitative TaqMan PCR was performed with commercially available assay-on demand probe primer sets for *p21* and *β-actin* (Applied Biosystems) and TaqMan Universal PCR Master Mix reagent according to the manufacturer's instructions. Reactions were performed using an Illumina Eco Real-Time PCR system. The expression levels of *β-actin* were used to normalize the relative expression levels of *p21*. The expression level of *p21* in L428$^{tetPU.1}$ cells before tetracycline removal was set to 100.

Western blot analysis

Cell lysates were resolved by SDS-PAGE and transferred onto nitrocellulose membranes. The membranes were incubated with anti-PU.1, anti-p21$^{WAF/CIP1}$, and antiactin primary antibodies (Santa Cruz Biotechnology) for 3-12 hours. Membranes were then incubated with peroxidase-labeled secondary antibodies for 30 minutes and developed using an enhanced chemiluminescence system (GE Healthcare).

Generation of L428$^{tetPU.1}$ cells stably expressing p21 siRNA

siRNA expression vectors were generated by insertion of annealed oligonucleotides targeting p21 and scrambled control siRNAs into the *BamHI* and *Hin*dIII sites of pRNA-U6.1/Zeo or pRNA-U6.1/ Hygro (GenScript).[27] siRNA expression vectors were transfected into L428$^{tetPU.1}$ cells by electroporation, and stable transformants were obtained by selection with zeocin (400 μg/mL) or hygromycin (200 μg/mL).

Detection of apoptosis

For detection of apoptosis, cHL cells were stained with an annexin V Phycoerythrin or Allophycocyanin Apoptosis Detection kit (Medical and Biologic Laboratories). Cells were analyzed using a FACSCalibur flow cytometer (Becton Dickinson).

Cell-cycle analysis

L428$^{tetPU.1}$ and KM-H2$^{tetPU.1}$ cell-cycle profiles were analyzed by staining with bromodeoxyuridine (BrdU) and 7-aminoactinomycin D (BrdU Flow Kits; BD Biosciences PharMingen),[28] 3 days after tetracycline withdrawal. Cells were analyzed by flow cytometry (FACSCalibur).

Results

PU.1 is down-regulated in Hodgkin lymphoma by methylation of the promoter and a −17 kb URE of the PU.1 gene

Previous studies have shown that PU.1 is generally highly down-regulated in both Hodgkin lymphoma cell lines and primary Hodgkin lymphoma cells.[23] In these studies, methylation-specific PCR revealed that the *PU.1* promoter is methylated, leading to

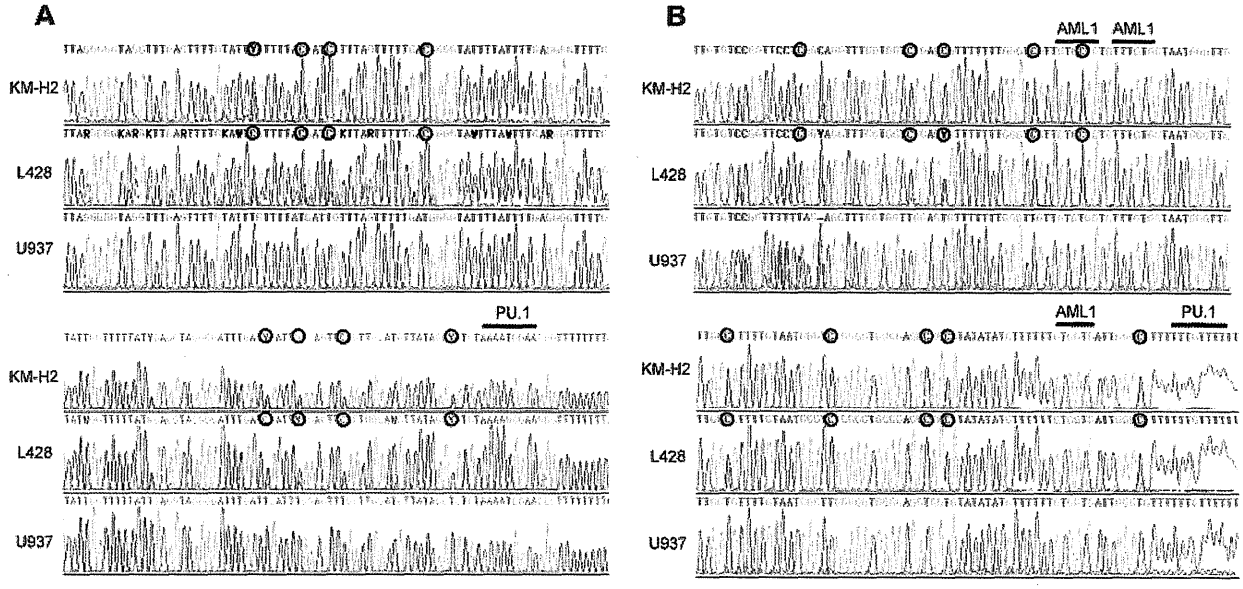

Figure 1. The promoter region and the −17 kb URE of the *PU.1* gene are highly methylated in cHL cells. (A) Bisulfite sequencing confirmed that the promoter of *PU.1* is highly methylated in L428 and KM-H2 Hodgkin lymphoma cell lines. ○ represents methylated cytosines. Underlining indicates the PU.1 binding site downstream of the translation initiation site. (B) Bisulfite sequencing revealed that the −17 kb URE was highly methylated in L428 and KM-H2 Hodgkin lymphoma cell lines. ○ represents methylated cytosines. Underlining indicates 3 RUNX1 (AML1) binding sites and a PU.1 binding site.

down-regulation of PU.1 expression. We previously demonstrated that PU.1 is strongly down-regulated in myeloma cell lines and the *PU.1* promoter was highly methylated as shown by bisulfite sequencing.[20] To confirm this mechanism of PU.1 down-regulation in Hodgkin lymphoma, we conducted bisulfite sequencing of the *PU.1* promoter region in the Hodgkin lymphoma cell lines, L428 and KM-H2. As shown in Figure 1A, the *PU.1* promoter region was heavily methylated in both cell lines, and there was no C-T conversion in CpG islands after bisulfite treatment of genomic DNA. Gene expression often requires *cis*-elements located > 10 kb or, in some cases, more than several hundred kilobases upstream of the transcriptional start site or downstream of the transcriptional termination site.[29-36] The expression of PU.1 also requires a URE located −14 kb and −17 kb upstream of its promoter in mice and humans, respectively.[18,19,21,22] Previously, we reported that PU.1 is down-regulated in multiple myeloma cells via methylation of its promoter and the −17 kb URE.[20] We therefore evaluated the methylation status of the −17 kb URE of *PU.1* in L428 and KM-H2 cells. The −17 kb URE of *PU.1* was highly methylated in both L428 and KM-H2 cells, indicating that PU.1 is silenced in cHL cells via methylation of both the promoter and the −17 kb URE (Figure 1B).

PU.1 induces growth arrest and apoptosis of Hodgkin lymphoma cell lines, L428 and KM-H2

We next evaluated whether down-regulation of PU.1 may play a role in Hodgkin lymphoma cell growth. We generated Hodgkin lymphoma cell lines that conditionally express PU.1 using a tet-off system, designated L428$^{tetPU.1}$ and KM-H2$^{tetPU.1}$. After the removal of tetracycline from growth medium, PU.1 was highly up-regulated in both L428$^{tetPU.1}$ and KM-H2$^{tetPU.1}$ cell lines (Figure 2A). Conditional expression of PU.1 induced complete growth arrest of both L428$^{tetPU.1}$ and KM-H2$^{tetPU.1}$ cells over the course of 7 days (Figure 2B-C). Cell-cycle analysis using BrdU and 7-aminoactinomycin D staining revealed that induction of PU.1 led to a decrease in S phase cells in both L428$^{tetPU.1}$ (15.8% vs 1.4%) and KM-H2$^{tetPU.1}$ cells (32.1% vs 9.9%) after 3 days, suggesting that PU.1 induced G_1 arrest in these cells (Figure 2D). We also observed an increase in the sub-G_1 population in both L428$^{tetPU.1}$ and KM-H2$^{tetPU.1}$ cells. Consistent with these data, annexin V staining revealed that PU.1 expression led to a significant increase in apoptotic cells in L428$^{tetPU.1}$ and KM-H2$^{tetPU.1}$ cells at day 3 (28.5% vs 72.9% and 17.1% vs 81.7%, respectively; Figure 2E). Morphologically, L428$^{tetPU.1}$ cells expressing PU.1 were enlarged and displayed numerous cell processes and vacuoles of various sizes, which in some cases occupied the majority of the cellular mass and nuclear compartment (Figure 2F). In addition, a number of L428$^{tetPU.1}$ PU.1-expressing cells exhibited nuclear fragmentation, a typical feature of apoptosis (Figure 2F). In comparison, KM-H2$^{tetPU.1}$ cells expressing PU.1 contained relatively smaller vacuoles, and many cells exhibited nuclear condensation, which is also a feature of apoptotic cells. These data demonstrate that PU.1 induces complete growth arrest and apoptosis in L428 and KM-H2 cells.

PU.1 induces growth arrest, regression of subcutaneous tumors, and prolonged survival in a Hodgkin lymphoma xenograft mouse model

We next investigated the role of PU.1 in a xenograft model of Hodgkin lymphoma. A total of 7×10^6 L428$^{tetPU.1}$ or KM-H2$^{tetPU.1}$ cells were injected subcutaneously in *Rag2*$^{-/-}$*Jak3*$^{-/-}$ *balb/c* mice, and tumors were grown to 1- to 2-cm in diameter. Mice were then divided into 2 treatment groups: one group continued drinking tetracycline-treated water (n = 8), whereas the other group was given nontreated water (n = 8). In mice taking tetracycline, tumors continued to grow and increase in size (Figure 3A-B), and a number of mice developed skin ulcers possibly induced by tumor necrosis. In contrast, tumors in mice given nontreated water ceased to grow and decreased in size in several cases (Figure 3C-D). All mice injected with L428$^{tetPU.1}$ or KM-H2$^{tetPU.1}$ cells, taking tetracycline, died within 96 days or 143 days, respectively. In contrast, more than 50% of mice without tetracycline survived > 200 days in both xenograft models. Furthermore, mice given nontreated water and harboring tumors < 1 cm in diameter had a 100%